



HAL
open science

Quantifying porosity changes in solid biomass waste using a disruptive approach of water retention curves (WRC) for dry anaerobic digestion

M.A. Hernández-Shek, M. Mathieux, Laura André, P. Peultier, A. Pauss,
Thierry Ribeiro

► To cite this version:

M.A. Hernández-Shek, M. Mathieux, Laura André, P. Peultier, A. Pauss, et al.. Quantifying porosity changes in solid biomass waste using a disruptive approach of water retention curves (WRC) for dry anaerobic digestion. *Bioresource Technology Reports*, 2020, 12, pp.100585. 10.1016/j.biteb.2020.100585 . hal-03246805

HAL Id: hal-03246805

<https://hal.science/hal-03246805v1>

Submitted on 7 Nov 2022

HAL is a multi-disciplinary open access archive for the deposit and dissemination of scientific research documents, whether they are published or not. The documents may come from teaching and research institutions in France or abroad, or from public or private research centers.

L'archive ouverte pluridisciplinaire **HAL**, est destinée au dépôt et à la diffusion de documents scientifiques de niveau recherche, publiés ou non, émanant des établissements d'enseignement et de recherche français ou étrangers, des laboratoires publics ou privés.



Distributed under a Creative Commons Attribution - NonCommercial 4.0 International License

1 **Quantifying porosity changes in solid biomass waste using a disruptive** 2 **approach of water retention curves (WRC) for dry anaerobic digestion**

3 M.A. Hernandez-Shek^{a,b,c}, M. Mathieux^{a,b}, L. André^a, P. Peultier^c, A. Pauss^b, T. Ribeiro^{a*}

4 ^aInstitut Polytechnique UniLaSalle, EA 7519 Transformations & AgroRessources, Rue Pierre Waguet, BP 30313,
5 F-60026 Beauvais Cédex, France.

6 ^bAlliance Sorbonne Université, EA 4297 TIMR UTC/ESCOM, Université de technologie de Compiègne, 60203
7 Compiègne cedex, France.

8 ^cEasymetha, 6 rue des Hautes Cornes, 80000 Amiens, France.

9
10 *Corresponding author: Thierry Ribeiro; Tel.: +33 (0) 344 06 76 11; E-mail: thierry.ribeiro@unilasalle.fr

11 **Abstract**

12 Knowledge of the porosity distribution of biomass is crucial to understand the liquid flow through porous
13 solid biomass treated in dry anaerobic digestion (D-AD). In this study, a novel adaptation of Water
14 Retention Curve (WRC) analysis was validated to characterize the pore distribution of representative
15 lignocellulosic biomasses; Cattle Manure (CM), roadside grass and corn stover. WRC analysis is
16 composed of a drainage analysis (DA) and thermogravimetry analysis (TGA). Macro, meso and
17 micropores values ranged from 33 to 63%, 25 to 44% and 7 to 16% for listed raw biomasses.
18 Additionally, changes in porosity distribution of CM treated in sacrificed Leach-Bed Reactor (LBR)
19 were quantifying; macropore volume decreased from 30.4 to 1.7% with the fiber degradation reducing
20 considerably the permeability and increasing the solid bed compaction. The findings of this study suggest
21 that the daily recirculated liquid volume could be progressively adapted considering the physical
22 evolution of the solid bed.

23 **Keywords**

24 Water retention curve; Porosity distribution; Dry anaerobic digestion; Solid biomass; Leach-bed
25 reactor

26

27 Nomenclature

BMP	Biochemical methane potential (NmL CH ₄ g _{VS} ⁻¹)
CCS	Chopped corn stover
CFD	Computational fluid dynamics
CHP	Combined heat and power
CM	Cattle manure
DA	Drainage analysis
D-AD	Dry anaerobic digestion
DM	Dried matter
DW	Drained water (kg)
I&S	Immersion and saturation
I/S	Ratio inoculum VS /substrate VS
K	Hydraulic conductivity (m s ⁻¹)
LBR	Leach-bed reactor
MIM	M-mobile/IM-immobile
PWP	Permanent wilting point
RSG	Roadside grass
S-CM	Shredded cattle manure
SW	Stagnant water (kg)
TGA	Thermogravimetry analysis
TS	Total solids (%)
VS	Volatile solids (% _{TS})
W ₀	Initial water content in the sample (kg)
W _{added to I&S}	Added water to immersion and saturation (kg)
WHC	Water-holding capacity (g _{water} g _{DM} ⁻¹)
WMB	Water mass balance (%)
WRC	Water retention curve
ε _{dry}	Dry porosity (%)
ε _{wet}	Wet porosity (%)
θ _{immobile}	Immobile water volume (L)
θ _{mobile}	Mobile water volume(L)
θ _{total}	Volumetric total water (L)
ρ _{dry}	Dry bulk density (kg m ⁻³)
ρ _{wet}	Wet bulk density (kg m ⁻³)

28

29

30 **1. Introduction**

31 Dry Anaerobic Digestion (D-AD) has already proven its efficiency in the methane recovery
32 from lignocellulosic biomass having more than 15% of Total Solids (TS) content (Ge et al.,
33 2016; Karthikeyan and Visvanathan, 2013; Rocamora et al., 2020). Accessibility and availability
34 of biomass are related to the cost of collection and transportation. Biomass with higher
35 concentration of TS involves lower transportation costs per unit of solids compared to low TS
36 feedstocks (Brown et al., 2012). Agricultural residues, such as cattle manure and corn stover are
37 the most common substrates for D-AD process in France (FranceAgrimer, 2016). Furthermore,
38 yard waste, which includes grass, is a major biowaste generated from municipalities, which has
39 become an interesting substrate for D-AD (Koch et al., 2010).

40 Given its simplicity and the physical characteristics of solid biomass, Leach-Bed Reactor (LBR)
41 operated in batch is the most common technology for the anaerobic treatment and valorization
42 of solid biomass (Riggio et al., 2017b). In this reactor, the solid biomass is irrigated with a
43 liquid inoculum -named leachate percolating the solid bulk until being recovered at the reactor
44 bottom. Liquid recirculation has a positive effect on the methane production, it improves the
45 contact between the microorganisms and the solid substrate and avoid possible failures by
46 diluting inhibitory compounds (Degueurce et al., 2016b; Kusch et al., 2012; Shahriari et al.,
47 2011). Despite the positive effect of liquid recirculation on biogas production (Degueurce et al.,
48 2016b; Kusch et al., 2012), there is no clear consensus between the parameters leading liquid
49 recirculation. In general, once an operation mode is chosen (total volume, frequency, flow), this
50 would be kept until the end of the batch operation.

51 Liquid percolation through the solid bed is feasible due to its porosity (Valencia et al., 2008).
52 The total porosity of a matrix represents the fraction not occupied by solid and which is
53 available for the liquid and gas phases. Porosity has been identified as a major element
54 influencing the liquid distribution and the degradation efficiency of biomass in LBR (Myint and

55 [Nirmalakhandan, 2008](#)). Despite the importance of biomass porosity and its evolution through
56 D-AD process, its analysis is poorly documented in literature. The physical changes of the solid
57 bed like the loss of permeability limit the efficiency of liquid percolation to maintain the solid
58 degradation ([André et al., 2015](#)). Unfortunately, to our knowledge, there is no method able to
59 efficiently describe the changes in porosity distribution of the solid bed. As consequence, daily
60 recirculated liquid volume still being established without considering the physical evolution of
61 the solid phase.

62 Pore media is frequently studied by its physical relation with water ([Gerke and Van Genuchten,](#)
63 [1993](#)). Initially developed for the analysis of soils, two-region MIM (M-mobile/IM-immobile
64 water) model has allowed the modeling of successive percolation and drainage operations and
65 the presence of non-uniform flow pathways in cattle manure ([André et al., 2015; Shewani et al.,](#)
66 [2015](#)). This model considers as mobile water the one present in the macropores and that drains
67 rapidly into the solid bed, while water retention is assured by the micropores (immobile water).
68 MIM model does not consider capillary region or mesopores, being this one of the highest
69 drawbacks in its application to porous media. As a consequence, capillary effects have been
70 responsible for differences between the experimental and numerical analysis of percolation
71 operations in LBR treating cattle manure. Meaning the importance of considering capillary
72 pores (mesopores) as an intermediate pore size between the macropores and the micropores.
73 Furthermore, thermogravimetric analysis (TGA) has been used for determining the free and
74 bound water present in biomass ([Dumas et al., 2015; Garcia-Bernet et al., 2011](#)). Some other
75 studies have focused only on the Water-Holding Capacity (WHC) of biomass without
76 considering the pores fraction responsible for water retention ([Fernandez et al., 2020; Sanchez et](#)
77 [al., 2019](#)).

78 Biomass porosity distribution and its evolution through D-AD process remains an open
79 question, limiting the D-AD process optimization and the liquid recirculation operation. Thus,

80 new methodologies need to be adapted and developed for solid biomass analysis. The Water
81 Retention Curve (WRC) analysis is a technique relating the soil water content with the matric
82 suction (Du, 2020; Wassar et al., 2016). This is a method frequently used to estimate the water
83 distribution and hysteresis in soils (hygroscopic water, the capillary water and the gravitational
84 drained water) thereby fixing water irrigation operations according to the soil type, the season
85 and the crop water necessities. The WRC of soils is built using pressured systems as the
86 Richards chambers or the sand pressure tables (Darwish, 2009; Jordan and Cerdá, 2010; Lavelle
87 et al., 2014; Menéndez et al., 2005). Hitherto, no application of WRC methodology has been
88 documented in literature for biomass, this could be explained by the fact that existed pressured
89 chambers do not correspond to the needed volume for biomass analysis.

90 The aim of this work was to present a novel adaptation of WRC methodology to quickly and
91 efficiently determine the pore distribution of solid biomass. This approach was inspired by the
92 analysis of soils, allowed to determine the macro, meso and micropores of porous medium
93 (Luxmoore, 1980). It integrates a first phase of immersion / saturation (I&S) of the sample with
94 water, followed by drainage analysis (DA) and finally the thermogravimetry analysis (TGA). In
95 the first part of this work, WRC methodology was used to characterize the pore distribution of
96 four of the most common lignocellulosic biomasses used as substrate in D-AD; Cattle Manure
97 (CM), Shredded Cattle Manure (S-CM), Chopped Corn Silage (CCS) and Roadside Grass
98 (RSG). Additionally, bulk density, WHC and permeability of biomasses were determined for
99 each biomass. Secondly, pores distribution evolution was determined from digested CM from
100 four LBR's of 60L started up in parallel and sacrificed at different stages of the D-AD process
101 (10, 15, 21 and 31 day). Changes in porosity distribution, fiber content of the solid phase and
102 permeability values were quantifying and correlated. The impact of porous changes over the
103 management of the liquid recirculation during the batch and methane production in LBR are
104 also discussed.

105

106 **2. Materials and Methods**

107 *2.1 Tested materials*

108 Biomass samples were collected in summer to avoid any variability due to seasonality following
109 the protocol described by Gy (1998). No conservation of samples was undertaken, these were
110 analyzed the same collection day.

111 *i. Cattle Manure (CM)*

112 CM is a mixture of cow slurry with the bedding material which is in most cases wheat straw.
113 Two kinds of CM, non-shredded CM and Shredded CM (S-CM) were respectively collected
114 from the farm of the Institute LaSalle Beauvais and from another farm located in Talmas
115 (France). Non-shredded CM presented fibers of wheat straw < 20 cm. Otherwise, industrially
116 size reduction enhanced fibers with less than 5 cm length in S-CM

117 *ii. Chopped Corn Stover (CCS)*

118 CCS is used as animal feed in farms. Silage fermentation of stored CCS could reduce its
119 nutritional value, then this is considered as a farm waste needed treatment, a sample of wasted
120 CCS was collected from the farm located in Beauvais. CCS particles have a cylindrical shape
121 and sizes between 1.0 and 2.0 cm length.

122 *iii. Roadside Grass (RSG)*

123 RSG recently harvesting by cutting machines was collected in Beauvais (France). RSG was still
124 green and fresh at the moment of collection. It was composed of fibers between 10 and 15 cm in
125 length and <3 mm of thickness.

126 2.2 Analytical methods

127 2.2.1 Biomass physicochemical characterization

128 For all the experiments, the total solids (TS) and volatile solids (VS) of the raw and
129 anaerobically digested biomass were determined (APHA, 2017). Dry and wet bulk density was
130 determined using the mass-volume ratio in a cylindrical shape. Total dry (ϵ_{dry}) and wet
131 porosities (ϵ_{wet}) were measured by dividing the saturated water by the total dry and wet sample
132 weight as following (André et al., 2015; Lam et al., 2008b):

$$\epsilon_{dry} = \frac{\text{Added water to fully saturate } (W_{sw})}{\text{Weight of dry sample } (W_d)} \quad (1)$$

$$\epsilon_{wet} = \frac{\text{Added water to fully saturate } (W_{sw})}{\text{Weight of wet sample } (W_w)} \quad (2)$$

133 Van Soest fractionation allowed the determination of the hemicellulose, cellulose and lignin
134 content (Van Soest, 1963). The biochemical methane potential (BMP) of the biomass was also
135 measured following the methodology proposed by (Holliger et al., 2016). Experimental data will
136 be presented as average values, in addition, the standard derivation of the results will be shown
137 as well.

138 2.2.2 Water Retention Curve (WRC) Analysis

139 Adapted from the analysis performed using the Richard's chambers to determine the porosity
140 distribution and the field capacity in soils (Darwish, 2009; Klute, 1986; Richards, 1948). The
141 proposed approach integrates a first stage of immersion and water saturation of the biomass
142 (I&S), followed by a second stage of drainage analysis (DA) and finally, the last stage of
143 evaporation of residual water and measurement by thermogravimetry (TGA) (Fig. 1). DA and
144 TGA allowed the quantification of water stocked in the different pores of the solid, Luxmoore,
145 (1980) pore size classification and definitions were considered in this work, macropores would
146 consider the pores larger than 1 mm, mesopores from 10 μm to 1 mm and micropores inferior to
147 10 μm . The determination of the different volumetric fractions satisfied the following equation:

$$\%Macropores + \%Mesopores + \%Micropores + \%Solids = 100\% \text{ volume} \quad (3)$$

148 Pore distribution tests were performed in duplicate for each biomass, except the sample of CM
149 which analysis was performed on four occasions to better statistical analysis and
150 representativeness of the proposed methodology.

151 *2.2.2.1 Sample preparation*

152 The medium to be analyzed is gently placed in a cylindrical plastic laboratory constructed
153 permeameter (internal diameter 0.26 m, total height 0.25 m) until reaching about 0.2 m solid
154 height. In order to avoid sample volume changes during the next step, the initial sample volume
155 was fixed using a metallic aperture grill on the top of the sample.

156 *2.2.2.2 Immersion and Saturation (I&S)*

157 Tap water was gently injected from the bottom until the solid bed was completely filled with
158 water. When water levels decreased for biomass absorption, more water was added until the top
159 grill. At this stage wet porosity was determined using Eq. 2. The system was maintained closed
160 for two hours to make the wetting and saturation process more efficient (Fernandez et al., 2020;
161 Shewani et al., 2015). At this stage, it is assumed that total biomass porosity was completely
162 filled with water, and biomass achieved the maximum WHC.

163 *2.2.2.3 Draining analysis (DA)*

164 Once the submerged time ended, water was gravitationally drained from the permeameter
165 bottom for 24 h. Drained water mass was measured using a HD150 balance (My Weigh, United
166 States, precision ± 20 g). The weight values were taken every 5 seconds during the first minute
167 and then every minute until completing the first 10 minutes of DA. From this moment, data was
168 registered each 10 min until the first hour and from there each hour to the end of the DA.
169 Disruption of linear behavior of recovered water with time in the DA indicated the limit between
170 the macropores and the rapid mesopores. According to Luxmoore (1980) in macropores
171 drainage may occur very rapidly with the presence of surface ponding or perched water, while

172 rapid mesopores or capillary flow may occur without the of these last. Thus, once the slope of
173 drainage drastically changed, the recovered water concerned rapid mesopores flow.

174 2.2.2.4 Thermogravimetric analysis (TGA)

175 Once the previous test was achieved, 20 g of remaining solid was collected and placed on an
176 aluminum pan (diameter 10 cm). Then, the sample was introduced into a moisture weight Mark
177 160Top-Ray (BEL Engineering). Water evaporation was carried on at 105°C and sample weight
178 loss data were registered each second using a RS232 port connected to a PC (Dumas et al.,
179 2015; Garcia-Bernet et al., 2011). Samples weight data was analyzed using the moisture
180 derivation of the Savitzky-Golay filter in Scilab 6.0 (Savitzky and Golay, 1964). This derivation
181 allowed to identify the limit between the water present in mesopores and water present in the
182 micropores of biomass. The Savitzky-Golay filter derivative of the resulted curve from the
183 evaporation test of the RSG sample is illustrated in Fig. 2. At first, a period of increasing
184 temperature is depicted until α , this is succeeded by a constant water evaporation until β , the
185 fraction of water evaporated since the beginning of the test until β refers to water presented in
186 capillary or mesopores.

187 2.2.3 Water mass balance in WRC analysis

188 Draining and evaporation test results allowed the construction of the experimental WRC for
189 each biomass; DA allowed the quantification of water present in macropores and in rapid
190 mesopores, whereas the TGA allowed the quantification of water stocked in capillaries
191 (mesopores) and water very attached to the biomass, these pores spaces were considered as
192 micropores. Water mass balance analysis was used to validate the results of WRC methodology
193 using the following equations:

$$\% \text{ Water mass balance (WMB)}: \frac{\text{Drained water (DW)} + \text{Stagnant water (SW)}}{\text{Water in sample (W}_0\text{)} + \text{Added water (W}_{\text{added to I\&S}}\text{)}} \quad (4)$$

194 With:

195 *Water in sample* (W_0): initial water weight in the sample determined by multiplying the
196 initial biomass weight by the humidity.

197 *Added water* ($W_{added\ to\ I\&S}$): added water to achieve immersion and saturation of the sample

198 *Drained water* (DW): drained water weight once DA is complete (Macropores and rapid
199 mesopores volume)

200 *Stagnant water* (SW): water present in the samples after DA determined by multiplying the
201 remaining mass by the humidity determined by TGA (Slow mesopores and micropores volume)

202 2.2.4 *Determination of Mobile and immobile water volume fractions*

203 In this work mobile (θ_{mobile}) and immobile ($\theta_{immobile}$) water volume fractions were determined
204 from the previous mass balance. These fractions have been determined from the total and added
205 water to achieve I&S.

$$\frac{\theta_{mobile}}{\theta_{added}} = \frac{DW}{W_{added\ to\ I\&S}} * 100 \quad (5)$$

$$\frac{\theta_{immobile}}{\theta_{added}} = \frac{W_{added\ to\ I\&S} - DW}{W_{added\ to\ I\&S}} * 100 \quad (6)$$

$$\frac{\theta_{mobile}}{\theta_{total}} = \frac{DW}{W_{added\ to\ I\&S} + W_0} * 100 \quad (7)$$

$$\frac{\theta_{immobile}}{\theta_{total}} = \frac{SW}{W_{added\ to\ I\&S} + W_0} * 100 \quad (8)$$

206 2.2.5 *Hydraulic conductivity*

207 The permeameter described in section 2.2.2 was used to determine the permeability of each
208 sample. The same procedure of filling was performed and tap water was added until the
209 permeameter limit (0.25 m), then, water was allowed to percolate the sample and the changes in
210 water level with time were recorded using a cell phone (one plus 6.0). Video was analyzing
211 using DaVinci software in order to better estimate the time of the water descent. The following
212 equation allowed the determination of the water permeability ($m\ s^{-1}$).

$$K = \frac{H_{biomass}}{t} * Ln \left(\frac{h_{o_water}}{h_{f_water}} \right) \quad (9)$$

213 Where $H_{biomass}$ is the biomass height (m), t is the recorded time (s), h_{o_water} and h_{f_water} were the
 214 initial and the final water height respectively (m).

215 *2.3 Inoculum characterization*

216 Liquid inoculum was obtained from a previous D-AD cycle in a 500L batch digester fed with
 217 CM operated under mesophilic temperature (37°C) for two months. Thereafter, it was stored in
 218 drums at room temperature for one week. Before sampling for D-AD experiments, the inoculum
 219 was homogenized. TS content was measured at 1.9% and the VS averaged 42.5%_{TS}. The initial
 220 pH was 8.4 and the VFA/alkalinity ratio was measured at 0.125.

221 *2.4 Dry Anaerobic Digestion of CM in Sacrificed LBR's*

222 Given its highlighted importance in agricultural methane production, CM was chosen as a
 223 substrate for D-AD process to validate and compare the results of this study with literature. In
 224 order to follow physical changes of biomass with the already proposed WRC method. Four
 225 batch reactors with liquid recirculation were started in parallel, and each was sacrificed at
 226 different stages of degradation according to the typical biogas flow behavior in a batch D-AD
 227 digester treating CM (André et al., 2015). The first batch reactor corresponded to the initial
 228 conditions of the CM before anaerobic digestion (day_0). The second reactor corresponds to the
 229 first peak of methane production (day_10), third reactor corresponds to the methane production
 230 valley founded between days (day_15), the fourth reactor was sacrificed once reaching the
 231 second peak of methane production (day_21) and finally, the fifth reactor was sacrificed when
 232 biogas flow would decrease until the batch end (day_31).

233 The four reactors used in this study were made of polyethylene; the internal diameter and the
 234 total height were 39 cm and 50 cm, respectively, for a total volume of approximately 60 L. A
 235 mesh (5 mm holes) placed at the bottom avoided solid blockage of liquid phase pipes

236 recirculation. Twenty-one kilograms of CM were gently placed in the reactor using hands,
237 subsequently, 22 kg of inoculum (liquid phase) was added obtaining a ratio Inoculum/Substrate
238 (I/S) of VS content equal to 0.05.

239 Loaded reactors were hermetically sealed and a thermostatically controlled water bad allowed to
240 keep mesophilic temperature (37°C) during all the batch duration. Approximately 40 L of the
241 liquid phase was daily recirculated (2 min each 2 h with a flow rate of 100 L h⁻¹) using
242 MasterFlex peristaltic pumps. A valve in the liquid phase circuit enabled samples to be taken for
243 analysis. Biogas production was continually measured using drum gas meter TG5 (Ritter,
244 Germany), biogas composition (CH₄, CO₂ and H₂) was monitored daily by a MGA300 multi-gas
245 analyzer (ADC Gas Analysis Ltd, Hoddesdon, United Kingdom).

246 In order to follow and control the anaerobic digestion process, the liquid phase was sampled and
247 analyzed on a daily basis. The pH and the conductivity were measured using Mettler Toledo
248 (Switzerland) SevenEasyTM S₂₀. The buffer capacity and the volatile fatty acid concentration
249 (VFA) were determined by two acidification steps using sulphuric acid. The first acidification
250 down to pH 5.0 allowed the buffer capacity to be determined, and the second acidification down
251 to pH 4.4 allowed the quantity of volatile fatty acids to be determined. These analyses were
252 carried by means of an automatic titrator T₅₀ (Mettler Toledo, Switzerland).

253 Once each reactor was sacrificed, physical characterization of the solid phase was performed
254 according section 2.2.1. In order to minimize any structural changes of the samples for WRC
255 analysis, similar core drilling procedure performed in soils was used, representative sampling
256 amount (around 3 kg) of the solid was taken using a sharpened cylinder and carefully introduced
257 into the permeameter. Finally, Pearson linear correlation analysis was performed to assess the
258 significance and correlation between the pore distribution with TS content, VS content, the fiber
259 content, the bulk density and permeability.

260 3 Results and Discussion

261 3.1 Biomasses physical characterization

262 Physical properties of four of the most common biomasses treated by D-AD process were
263 measured in this section (**Table 1**). Physical properties such as the TS, the VS and the bulk
264 density are essential parameters for D-AD because they determine the loading of biomass, and
265 consequently the methane yield per volume of reactor (Caicedo et al., 2017; Møller et al., 2014).
266 For tested biomass, TS values ranged from 14.5 and 20.1 % except for corn silage with 37.7%
267 TS (**Table 1**). These values of TS are in the range of lignocellulosic biomass treated by D-AD
268 process (Brown et al., 2012; Rocamora et al., 2020; Sawatdeenarunat et al., 2015). Biomass is
269 considered as a spongy material; it means that according to their particle size, biomass can
270 integrate and absorb high water quantities inside the vegetal tissues, hence, dry biomass is
271 frequently used as bedding by livestock activities. Biomass WHC increase with size reduction
272 due to an increase of the contact surface of biomass (Dumas et al., 2015; Fernandez et al., 2020).
273 This fact was observed when comparing CM with S-CM, the WHC were 6.7 ± 0.2 and 7.4 ± 0.2
274 $\text{g}_{\text{water}} \text{g}_{\text{DM}}^{-1}$ respectively.

275 Bulk density and porosity depend on the particle shape, size and orientation, the particle specific
276 density, the particles size distribution, the moisture content and the applied pressure (Lam et al.,
277 2008a). In shredded CM, the fibers size reduction and a larger presence of feces increased the
278 humidity, as a consequence, higher wet and dry bulk density values compared to non-shredded
279 CM (**Table 1**). Initial bulk density has been identified as a key factor in the anaerobic treatment
280 of municipal solid waste in LBR, indeed, over 1000 kg m^{-3} inhibition of methane production
281 was observed (Caicedo et al., 2017). Degueurce et al., 2016a have reported similar values of
282 non-shredded CM bulk density for samples collected during the winter, they have used the
283 “Schaub-Szabo” device to measure the evolution of the bulk density with the material height

284 from 0.2 to 2.2 m, their results suggests an increase in bulk density from 311 to 577 kg m⁻³ with
285 the material deep, meaning an increase of 85% of the bulk density.

286 Biomass porosity values are shown in **Table 1**, the dry porosity concerns the total porosity after
287 drying the sample at 105°C, whereas the wet porosity refers to the total available porosity of the
288 sample at the moment it was collected. Total dry porosity values were around 90% for all
289 biomass, according to [Jordan and Cerdá \(2010\)](#), total porosity is very high over 60% and too
290 low under 30%. Similar values of dry bulk density and dry porosity have been presented by
291 [André et al. \(2015\)](#) treating non-shredded CM, however, values of dry porosity barely changed
292 between the initial CM and the digestate. In consequence, total dry porosity by itself does not
293 represent the physical changes of CM treated in D-AD.

294 Wet porosity values showed higher variability than dry, meaning that water presence and its
295 distribution may play an important role in the porosity volume of biomass and in the hydraulic
296 behavior. Initial moisture in biomass samples indicates that a portion of porosity is already water
297 filled. Comparing S-CM with non-shredded CM, size reduction enhanced important physical
298 changes in the biomass, reducing wet porosity values from $51.7 \pm 1.3\%$ to $18.6 \pm 1.7\%$.

299 Moreover, despite the differences in particle size and shape and TS content, CCS and RSG
300 presented similar values of porosity and bulk density, both dry and wet. Based on the previous
301 results, it appears that physical parameters present a high variability given their interdependent
302 correlation, more research should be performed in order to establish detailed physical models
303 than the existed ones to easily determine the potential biomasses that could be treated in LBR
304 for methane recovery.

305 *3.2 WRC analysis of biomass for pores distribution determination*

306 As describe before, total porosity can be distinguished according to its function and relation with
307 water (**Fig. 1**); macropores are the larger ones and allow the rapid percolation of water and the
308 presence of a gas phase in the biomass. Next, the mesopores ensure the presence of capillary

309 water, they can be divided into rapid and slow mesopores. Finally, the micropores water volume
310 concerns vicinal or bound water. Water stocked in mesopores can be removed by mechanical
311 dewatering, whereas the water in the micropores can be only withdrawn using heat. **Fig. 3**
312 illustrates the experimental WRC for each tested biomass, this analysis is composed of two sub-
313 sequential analyses; the DA and the TGA giving as result the porosity distribution for each
314 biomass, macro-, meso-, micropores and solid percentages of the total biomass bulk volume.
315 Macropores were represented with green color, mesopores with yellow, micropores in blue and
316 solid fraction in gray.

317 *3.2.1 DA: Macropores and rapid mesopores volumes*

318 According to the proposed WRC methodology, the water volume present in macropores
319 channeling would flow with a linear behavior in the first seconds of the DA, a change in this
320 linear behavior indicates the macropores water stock depletion, from this point, recovered water
321 in the next hours for DA concerns the water stocked in rapid mesopores channeling (dash yellow
322 line). According to [Luxmoore \(1980\)](#), macropores drainage occurs very rapidly once DA start,
323 while, rapid mesopores drainage includes slow capillary water flow without the presence of
324 ponding or perched water in the solid. The DA was maintaining for 24 hours in order to ensure
325 maximal water recovery from rapid mesopores. Time log-scale was useful to represent the
326 draining behavior since higher changes are expected in the first minute of the test.

327 Similar values of macropores volume for CCS and RSG were measured, 58.0% and 62.0%
328 respectively (**Fig. 3a** and **b**). However, the draining was faster for the RSG than for the CCS,
329 this explains the slight difference between the macropores slopes of these two biomasses. Even
330 if these samples have similarities in their physical properties, the solid particle shape is different
331 affecting the shape of pores, as a consequence, differences in the drainage velocity have been
332 observed. Further research is necessary in order to fully determine the effect of particles shape
333 on the pores shape structure for solid biomass. Otherwise, WRC results of S-CM presented low

334 macropore volume (1.1%) affecting the amount of water recovered in DA (**Fig. 3d**). Contrary to
335 S-CM (**Fig 3c**), non-shredded CM had better macropores structure with 30.4%. As indicated
336 before, rapid mesopores volume was determined after the linear macropores draining for each
337 biomass, for RSG, CCS and CM, the rapid mesopores volume was 7.9%, 8.43% and 5.32%
338 respectively, whereas for S-CM only had 0.31% for this type of pore channeling.

339 The presence of macropores is linked with the permeability values of matter (**Table 1**). In
340 biomasses with lower values of macropores, lower values of permeability have been observed.
341 Considering the S-CM, the measured permeability value (**Table 1**) was only $1.2 \cdot 10^{-8} \text{ m s}^{-1}$, this
342 was very low compared to the other tested biomass with values from $8.6 \cdot 10^{-4}$ to $1.3 \cdot 10^{-3} \text{ m s}^{-1}$.
343 Concentrated biomasses with lower values than 10^{-4} as the S-CM could not be an indicated
344 substrate for D-AD process with liquid recirculation, because water can barely infiltrate the
345 biomass and very low percolation rate is observed. This kind of biomass could be subject better
346 of a reactor type different from LBR.

347 Finally, the DA allowed the determination of the WHC at 24 h of drainage of biomasses.
348 Compared to other biomasses, S-CM was the biomass with higher WHC value with $(7.4 \pm 0.2 \text{ g}$
349 $\text{water} / \text{g TS})$ (**Table 1**). WHC values for CM, RSG and CCS were 6.74, 7.35 and 4.08 $\text{g water} / \text{g}$
350 TS respectively. [Fernandez et al. \(2020\)](#) showed similar results of WHC for samples of CM
351 before and after industrial size reduction. Consequently, biomass WHC is affected by the same
352 parameters determining physical properties described before.

353 3.2.2 TGA: Slow mesopores and micropores volumes

354 The next step in the proposed methodology concerns the TGA, here a sample of the remained
355 solid of DA was analyzing using a thermogravimetric balance in order to quantifying the slow
356 mesopores and the micropores volume. Whilst the former refers to water trapped inside crevices
357 and interstitial spaces, the latter made emphasis on the hydration water (water chemically bound
358 to the particles) and the vicinal or surface water (monolayer and multilayer) ([Garcia-Bernet et](#)

359 [al., 2011](#)). The limit between mesopores and micropores for RSG sample is depicted in **Fig 2**.
360 The fraction of water evaporated since the beginning of the test until β refers to water presented
361 in capillary or mesopores which is less influenced by the solid particles. This fraction of water
362 plays a key role in D-AD since it determines the available water for microorganisms (Garcia-
363 Bernet et al., 2011). As can be seen, β mark a sudden change of the water evaporation derivative
364 at time 480 seconds, it means that the constant water rate evaporation ended and from this point
365 the remaining humidity is harder to evaporate, thus a reduction in the evaporation rate indicating
366 the limit between mesopores and micropores. Water evaporated from β to ψ is considered as
367 micropores volume water, given its strong relation with the solid, this water fraction is not
368 available from metabolic activities of microorganisms ([Abbassi-Guendouz et al., 2012](#); [Garcia-
369 Bernet et al., 2011](#)).

370 The results of TGA for each biomass are also depicted in **Fig. 3**. Total mesopores volume
371 fraction concerns the sum of the volume of rapid mesopores determined in DA and the slow
372 mesopores quantifying using the TGA. Similar values were obtained for the mesopores volume
373 of RSG and CCS with $26.4 \pm 0.8\%$ and $25.2 \pm 0.3\%$ respectively. In contrast, CM samples
374 presented more significant number of mesopores and micropores than RSG and CCS, the
375 presence of animal slurry would be responsible for these higher values. S-CM achieved $64.9 \pm$
376 3.6 of mesopores volume, while for CM this fraction represented $44.4 \pm 3.4\%$ of the total
377 porosity. As can be seen, in S-CM the macropores volume was transformed in mesopores
378 volume due to the size particles reduction. Mesopores volume could include dead-end pores and
379 isolated or closed pores of the solid volume ([Nishiyama and Yokoyama, 2017](#); [Yokoyama and
380 Takeuchi, 2009](#)), in these pores water and gas could be stocked and limited mass transfer may
381 enhance local inhibition of D-AD process .

382 Similarities between the values of solid and micropores volumes percentages for all biomasses
383 were observed (**Fig 2**), this could be explained due to micropores are inside the solid fraction

384 and on its walls surface; indeed, SEM images have already allowed the observation of the
385 internal micropore structure of wheat straw fibers (Han et al., 2012). In S-CM, size reduction
386 increased the microporosity volume by the creation of more surface of solid, thus higher WHC.
387 Otherwise, compared with the other tested biomasses, RSG obtained the lower value of
388 micropores 6.8% and solid volume fraction 4.8%, this could be due to that sample was analyzed
389 fresh and green, just after harvesting; thus, the vegetal structures were not degraded and were
390 naturally filled with water and less water absorption took place while the test was performed. It
391 seems that biomass sponginess increases by drying due to a partial irreversible collapse of pores
392 and the creation of larger water absorption pores (Meng et al., 2013).

393 3.2.3 WRC analysis Vs MIM model

394 In the double porosity MIM model, the volumetric water content is assumed to be divided into
395 two distinct volumetric regions; mobile (θ_{mobile}) also called macropores and immobile (θ_{immobile})
396 known as micropores. In order to compare WRC analysis with previous works using double
397 porosity model and setting the advantages of the proposed methodology, mobile (θ_{mobile}) and
398 immobile (θ_{immobile}) water volume fractions have been determined from the total water and the
399 added water to achieve I&S. $\theta_{\text{mobile}}/\theta_{\text{added}}$ refers to the drained water after 2 hours over the added
400 water, thus the sum of macropores and rapid mesopores volume, controversy, $\theta_{\text{immobile}}/\theta_{\text{added}}$
401 indicate the stagnant water fraction stocked in slow mesopores and microporosity over the added
402 water.

403 Analysis of CM gave as results $60.0 \pm 3.6\%$ of $\theta_{\text{mobile}}/\theta_{\text{added}}$ and $40.0 \pm 3.6\%$ of $\theta_{\text{immobile}}/\theta_{\text{added}}$;
404 similar values were reported by André et al. (2015) as macro and microporosity, 64% and 36 %
405 respectively, using modeling of tracer tests. MIM model limitations have been observed since it
406 does not consider the initial absorbed water by the sample before the test in which diffusion and
407 convection of the tracer is more difficult. As a consequence, inconsistent results in the first 21
408 days of D-AD process indicates difficulties in determining the pore distribution of digested

409 samples of CM. In WRC analysis, the initial volumetric was including in the mesopores and
410 micropores volume calculation, this could represent an advantage over MIM model.

411 In another work, [Shewani et al. \(2015\)](#) using double region porosity model have measured
412 values from 18 to 50% for macroporosity, 42 to 70% for microporosity and 8 to 12% for the
413 solid volume of CM with different compaction levels. In this work, using the same calculation
414 proposed by the previous authors for CM with 18.59 ± 0.43 %TS, values in the same range of
415 measure were determined at 30.5 %, 60.5% and 9% respectively for macroporosity,
416 microporosity and solid volume, Even though [Shewani et al. \(2015\)](#) have for the first time given
417 values for macropores, micropores and solid volume, their method for porosity distribution
418 does not consider the mesopores or capillary volumes. Consequently, this fraction of pores was
419 responsible for differences between experimental and calculated drainage results using
420 Computational Fluid Dynamic (CFD) tool. The proposed WRC analysis included the mesopores
421 or capillary volume and offer a better pore distribution information for future studies of these
422 kinds of porous media.

423 In order to measure the applicability and accuracy of WRC analysis to determine the water
424 distribution in biomass samples, water mass balances (WMB) were performed using Eq. 4 (see
425 **Table 1**) obtaining higher values than $96.7 \pm 0.1\%$. WRC methodology coupled with tracer tests
426 and digital volumetric imaging could be powerful tools in the understanding of the pore
427 distribution network evolution of treated biomass in D-AD. Finally, the effect of pore
428 distribution, tortuosity and preferential flow pathways on liquid recirculation could be fully
429 simulated using CFD ([Vallabh et al., 2011](#)).

430 *3.3 Dry Anaerobic Digestion of CM in Sacrificed LBR*

431 In the previous section, the use of WRC analysis has successfully quantifying the pores
432 distribution of several biomasses. This section presents the results of the changes in porosity
433 distribution of anaerobically digested CM from days 10, 15, 21 and 31 have been sampled from

434 60 L sacrificed LBR's. Reactor mass balances between the inlet and the outlet ranged from
435 93.28% to 99.62% indicating a good D-AD experimental performance. The BMP value of CM
436 was measured at $222.8 \pm 4.4 \text{ NmL CH}_4 \text{ gVS}^{-1}$, this BMP was recovered at 98.66% on day 31.
437 Monitoring of the volatile fatty acids, pH and buffer capacity did not evidenced inhibition
438 problems during the D-AD process.

439 *3.3.1 Biogas Production*

440 Similar behavior on methane production was observed for the four LBR compared with
441 literature ([Degueurce et al., 2016c](#); [Riggio et al., 2017a](#)), **Fig. 4a** presents the biogas and
442 methane flow of the last reactor sacrificed at day 31. The first gas peak was observed around
443 day 3, this was mainly carbon dioxide produced by aerobic digestion of rapid fermentative
444 matter partially given the initial oxygen present in matter before the reactor sealing. Second gas
445 peak production was achieved for all reactors between days 9 and 11. The valley between peaks
446 2 and 3 mark the slack on methane production. The third and last gas production peak was
447 observed at day 16.5 ± 1.5 for the two remaining reactors. The cumulated methane for all
448 reactors and the average production at the sacrificed days of still working reactors is depicted in
449 **Fig. 4b**. Differences in methane production were attributed to the starting-up of the heating
450 baths at the first moment of the experiment and to the experimental uncertainties. The results of
451 methane production of these four LBR's were similar to the results presented by [André et al.](#)
452 ([2015](#)) using recirculation each 2 h during 2 min with 100 L h^{-1} of flow.

453 *3.3.2 Cattle Manure Physical Characterizations at Different Stages of D-AD*

454 Physical characterization of cattle manure at different stages of D-AD process included the TS
455 content, VS content, dry and wet bulk density and porosity and the WHC (**Table 2**). TS content
456 decreased from $18.59 \pm 0.43\%$ to $11.10 \pm 0.51\%$ between the initial CM and the digestate at 31
457 days. VS consumption presented a linear behavior with time, probably matter degradation would
458 have continued for some days more after day 31. Water impregnation and solid degradation

459 enhanced the augmentation of wet bulk density from 407.8 ± 14.1 to 914.2 ± 10.9 kg m⁻³, in
460 contrast, wet porosity values decreased from 51.7 ± 1.3 to 10.2 ± 1.5 % with time proving the
461 bulk compaction with D-AD process with liquid recirculation. Dry values of bulk density and
462 porosity did not present important changes as wet values (**Table 2**), thus water in samples plays
463 an important role in physical characterization of CM and digestates. Similar results were
464 obtained comparing the values of TS, VS, dry bulk density and dry porosity with the reported
465 values by [André et al. \(2015\)](#). Otherwise, similarities between the values of the wet bulk density
466 determined at the 60 L LBR's (data not shown) and those determined with the permeameter for
467 WRC methodology were observed, meaning that the use of a 13 L permeameter did not inflect
468 important changes in the structure of the digested biomass once this was sampled and placed in
469 the permeameter.

470 3.3.3 WRC and porosity distribution of CM at different stages of D-AD in sacrificed LBR

471 The WRC of CM and digested samples recovered at days 0, 10, 21 and 31 are depicted in **Fig.**
472 **5a**. In DA, the slope determining macropores in D-DA decreases with the anaerobic degradation
473 of the solid medium. Initially, the macropores slope value in DA was -0.09, this value gradually
474 decreased with the solid degradation, on day 10 the slope value was -0.059, at day 15 this was
475 determined at -0.056, at day 21 was -0.029 and finally at day 31 the slope value was reduced
476 until -0.006. Rapid mesopores (dashed yellow line) slopes presented lower variability than
477 macropores slopes, they changed from -0.006 and -0.004 from days 0 to 31. TGA's results are
478 also shown in **Fig. 5a**, as can be observed, the time of the test was slightly different for all
479 samples even if the sample amount was the same in all performed TGA. In samples at day 0, the
480 total humidity was removed in average 2865 seconds, this time increased at days 10 to 3150
481 seconds, degraded mater was able to hold more water, thus micropores volume increased from
482 $16.2 \pm 3.6\%$ to 21.1 ± 3.9 in the first 10 days. After this point, micropores volume remains
483 almost similar until the end of the experiment on day 31. Evaporation time was inferior on days

484 31 and 21, with 2670 and 2250 seconds, respectively. Moreover, water mass balance (Eq. 4)
485 values obtained for WRC analysis ranged from 88.3 ± 1.3 to 98.5 ± 2.2 % (**Table 2**), meaning a
486 good WRC analysis performance.

487 Volume porosity distribution changes are depicted in **Fig 5b**. Macropores decreased linearly
488 from 30 ± 3 on days 0 to $1.7 \pm 0.3\%$ on day 31, meaning a reduction of 94.3%. Macropores were
489 converted into mostly mesopore volume which increased linearly from 44.4 ± 3.4 to $65.4 \pm$
490 0.2% . Moreover, micropores volume slightly increased from 16.2 ± 3.6 to $22.9 \pm 0.3\%$. Previous
491 results drive to a group of linear regression equations able to estimate the volumetric fractions of
492 CM related in Eq. (3). **Table 3** shows the slope (m) and the y-intercept which represent the
493 initial percentages of macro, meso and micropores of CM. The use of these equations can allow
494 the estimation of pores distribution changes of anaerobically digested CM between 0 and 31
495 days in 60 L LBR.

496 *3.3.4 Effect of fiber degradation on pore distribution evolution and the permeability of the* 497 *solid bed*

498 In this section the structural changes of the solid phase were related with fibers biological
499 degradation. As defined before, CM is a mixture between cow feces and the wheat straw used as
500 bedding material. The presence of wheat straw fibers gives a solid structure and high porosity
501 values allowing the liquid percolation in LBR in the first days of batch. As a vegetal material,
502 wheat straw is composed of fibers of cellulose, hemicellulose and lignin. Fiber content has been
503 determined for samples from sacrificed D-AD reactors (**Fig. 6a**). Hemicellulose decreased from
504 27.2 ± 0.2 to 17.2 ± 0.6 %_{TS}, whilst cellulose decreased from 31.9 ± 1.2 to 22.9 ± 1.0 %_{TS}. The
505 lignin is a non-degradable molecule by D-AD, thus, increase of the lignin content in the solid
506 fraction was observed from 7.4 ± 0.2 % to 10.8 ± 0.5 %_{TS}. **Table 3** depicts the linear regression
507 parameters determining the kinetic degradation of hemicellulose and cellulose respectively,
508 similar patterns of biological degradation were observed for both.

509 According to the Pearson correlation results between the pore distribution changes with fiber
510 degradation and loss of permeability, macropores volume and the mass height were linearly
511 related to the degradation of cellulose and hemicellulose content of the biomass. Strong
512 correlations between these parameters were observed. Macropores reduction was correlated with
513 hemicellulose and cellulose degradation in 0.98 and 0.93 respectively with p-values inferior to
514 0.05 (**Table 4**). Moreover, fiber degradation was found responsible for the loss of solid
515 permeability from $2.5 \pm 0.2 \cdot 10^{-3}$ to $6.1 \pm 0.7 \cdot 10^{-5}$ m s⁻¹ (**Fig 6b**). The permeability was
516 reduced in 97.6%, which is a very approximate value of the macropores reduction of 94.3% in
517 31 days of D-AD treatment of CM. Similar permeability reduction behavior was observed by
518 [André et al. \(2015\)](#) in quantifying non-uniform flow using tracer experiments.

519 Methane production was well correlated with solid physical changes and fiber degradation with
520 Pearson coefficient values higher than 0.79. Macropores volume reduction was strongly related
521 to the settlement and compaction of the biomass with correlation coefficient of 0.98 (**Table 4**),
522 indeed, the CM height was reduced from 42 ± 2 to 18.0 ± 0.4 cm in LBR between days 0 to 31,
523 meaning height reduction of 57.1%. Hence, solid height decrease can be used as an indicator of
524 macropores and permeability reduction. This consideration is important since at the industrial
525 scale, following of the solid height would be easier than macropores and permeability;
526 additionally, this does not entail the reactor sacrifice necessarily for solid sampling.

527 *3.3.5 Implication of macropores reduction on the liquid recirculation operation in D-AD* 528 *process*

529 In literature the positive effect of liquid recirculation on biogas production in LBR is well
530 known ([Degueurce et al., 2016b](#); [Kusch et al., 2012](#)). However, there is no clear consensus
531 between the parameters leading liquid recirculation. In general, an operation mode is chosen
532 once (total volume, frequency, flow) and is kept until the end of the batch operation without
533 considering the physical changes occurred on the solid bed. [André et al. \(2015\)](#) has reported

534 poor percolation through the digestate on day 32, instead, liquid flow occurs at the reactor
535 boundary, which is useless to keep moisture content inside the solid bed and to maintain solid
536 degradation.

537 Since liquid percolation is possible due to the presence of macropores, the recirculated liquid
538 volume should be adjusted according to the macropores reduction. This could enhance important
539 reductions of energy consumption by recirculation pumps and extend their useful life period in
540 industrial biogas production. In this work, approximately 40 L of liquid was discontinuously
541 recirculated daily (2 minutes each 2 hours with flow 100 L/h), this recirculation mode was
542 chosen for several reasons: the first 40 L was the initial solid working volume in the reactor,
543 secondly, this recirculation mode has shown good D-AD performance for CM in previous
544 research works ([André et al., 2016, 2015](#)). An alternative pattern of recirculation is shown in **Fig**
545 **6c**, here the daily recirculated volume is reduced considering the loss of macropores. Hitherto,
546 none study about the effects of decreasing recirculation volume over D-AD has been found in
547 literature. In this type of recirculation, only the liquid volume able to pass through the solid bed
548 would be irrigated, avoiding excessive recirculation and liquid flow on the reactor boundary.
549 Thus, the recirculated volume could be reduced in 50% in around 15 days (**Fig 6c**), and
550 completely suppressed at day 31 in the treatment of CM.

551 **4 Conclusion**

552 D-AD using LBR system is often used in practice, while leaching pattern and strategy are not
553 well understood. Therefore, characterization of the pore in the digestion medium is required.
554 WRC analysis was useful to quantify the pore distribution of various raw solid biomasses into
555 macro, meso and micropores. Solid compaction and loss of permeability during CM batch
556 fermentation were related with the linear decrease of macropores and structural changes due to
557 lignocellulosic fiber degradation. As macropores are essential to ensure percolation of the liquid,

558 the recirculated volume could be progressively reduced considering the kinetics of macropores
559 volume decrease.

560 **5 Supplementary material**

561 Visual aspect of studied biomasses, liquid phase monitoring, reactor mass balances and Pearson
562 correlation coefficients can be consulted as supplementary material.

563 **6 Acknowledgments**

564 The authors wish to thank the Agence Nationale Recherche Technologie (ANRT) for the
565 financial support of this work and for the Ph.D. grant of Manuel HERNANDEZ-SHEK (CIFRE
566 n° 2017/0352).

567 **7 References**

- 568 Abbassi-Guendouz, A., Brockmann, D., Trably, E., Dumas, C., Delgenès, J.-P., Steyer, J.-P., Escudié, R.,
569 2012. Total solids content drives high solid anaerobic digestion via mass transfer limitation.
570 *Bioresour. Technol.* 111, 55–61. <https://doi.org/10.1016/j.biortech.2012.01.174>
- 571 André, L., Durante, M., Pauss, A., Lespinard, O., Ribeiro, T., Lamy, E., 2015. Quantifying physical
572 structure changes and non-uniform water flow in cattle manure during dry anaerobic digestion
573 process at lab scale: Implication for biogas production. *Bioresour. Technol.* 192, 660–669.
574 <https://doi.org/10.1016/j.biortech.2015.06.022>
- 575 André, L., Ndiaye, M., Pernier, M., Lespinard, O., Pauss, A., Lamy, E., Ribeiro, T., 2016. Methane
576 production improvement by modulation of solid phase immersion in dry batch anaerobic digestion
577 process: Dynamic of methanogen populations. *Bioresour. Technol.* 207, 353–360.
578 <https://doi.org/10.1016/j.biortech.2016.02.033>
- 579 APHA, 2017. Standard methods for the examination of water and wastewater, 23rd ed, American Public
580 Health Association. Inc. Washington, DC.
- 581 Brown, D., Shi, J., Li, Y., 2012. Comparison of solid-state to liquid anaerobic digestion of lignocellulosic
582 feedstocks for biogas production. *Bioresour. Technol.* 124, 379–386.
583 <https://doi.org/10.1016/j.biortech.2012.08.051>
- 584 Caicedo, L.M., Wang, H., Lu, W., De Clercq, D., Liu, Y., Xu, S., Ni, Z., 2017. Effect of initial bulk
585 density on high-solids anaerobic digestion of MSW: General mechanism. *Bioresour. Technol.* 233,
586 332–341. <https://doi.org/10.1016/j.biortech.2017.02.107>
- 587 Darwish, T., 2009. Caractérisation des propriétés hydrodynamiques d'un sol de la Bekaa (Liban) sur les

588 rives du fleuve Litani. *Étude Gest. des Sols* 16, 67–84.

589 Degueurce, A., Clément, R., Moreau, S., Peu, P., 2016a. On the value of electrical resistivity tomography
590 for monitoring leachate injection in solid state anaerobic digestion plants at farm scale. *Waste*
591 *Manag.* 56, 125–136. <https://doi.org/10.1016/j.wasman.2016.06.028>

592 Degueurce, A., Tomas, N., Le Roux, S., Martinez, J., Peu, P., 2016b. Biotic and abiotic roles of leachate
593 recirculation in batch mode solid-state anaerobic digestion of cattle manure. *Bioresour. Technol.*
594 200, 388–395. <https://doi.org/10.1016/j.biortech.2015.10.060>

595 Degueurce, A., Trémier, A., Peu, P., 2016c. Dynamic effect of leachate recirculation on batch mode solid
596 state anaerobic digestion: Influence of recirculated volume, leachate to substrate ratio and
597 recirculation periodicity. *Bioresour. Technol.* 216, 553–561.
598 <https://doi.org/10.1016/j.biortech.2016.05.113>

599 Du, C., 2020. A novel segmental model to describe the complete soil water retention curve from
600 saturation to oven dryness. *J. Hydrol.* 584, 124649. <https://doi.org/10.1016/j.jhydrol.2020.124649>

601 Dumas, C., Silva Ghizzi Damasceno, G., Abdellatif, B., Carrère, H., Steyer, J.P., Rouau, X., 2015.
602 Effects of grinding processes on anaerobic digestion of wheat straw. *Ind. Crops Prod.* 74, 450–456.
603 <https://doi.org/10.1016/j.indcrop.2015.03.043>

604 Fernandez, H.C., Ramirez, D.A., Franco, R.T., Buffière, P., Bayard, R., 2020. Methods for the evaluation
605 of industrial mechanical pretreatments before anaerobic digesters. *Molecules* 25, 1–14.
606 <https://doi.org/10.3390/molecules25040860>

607 FranceAgrimer, 2016. L'observatoire national des ressources en biomasse - Évaluation des ressources
608 disponibles en France. *Les études Fr.*

609 Garcia-Bernet, D., Buffière, P., Latrille, E., Steyer, J.P., Escudíé, R., 2011. Water distribution in
610 biowastes and digestates of dry anaerobic digestion technology. *Chem. Eng. J.* 172, 924–928.
611 <https://doi.org/10.1016/j.cej.2011.07.003>

612 Ge, X., Xu, F., Li, Y., 2016. Solid-state anaerobic digestion of lignocellulosic biomass: Recent progress
613 and perspectives. *Bioresour. Technol.* 205, 239–249. <https://doi.org/10.1016/j.biortech.2016.01.050>

614 Gerke, H.H., Van Genuchten, M.T., 1993. A dual-porosity model for simulating the preferential
615 movement of water and solutes in structured porous media. *Water Resour. Res.* 29, 305–319.
616 <https://doi.org/10.1029/92WR02339>

617 Gy, P.M., 1998. *Sampling for Analytical Purposes* 172.

618 Han, L., Feng, J., Zhang, S., Ma, Z., Wang, Y., Zhang, X., 2012. Alkali pretreated of wheat straw and its
619 enzymatic hydrolysis. *Brazilian J. Microbiol.* 43, 53–61. <https://doi.org/10.1590/S1517-83822012000100006>

620

621 Holliger, C., Alves, M., Andrade, D., Angelidaki, I., Astals, S., Baier, U., Bougrier, C., Buffière, P.,
622 Carballa, M., De Wilde, V., Ebertseder, F., Fernández, B., Ficara, E., Fotidis, I., Frigon, J.C., De
623 Laclos, H.F., Ghasimi, D.S.M., Hack, G., Hartel, M., Heerenklage, J., Horvath, I.S., Jenicek, P.,
624 Koch, K., Krautwald, J., Lizasoain, J., Liu, J., Mosberger, L., Nistor, M., Oechsner, H., Oliveira,

625 J.V., Paterson, M., Pauss, A., Pommier, S., Porqueddu, I., Raposo, F., Ribeiro, T., Pfund, F.R.,
626 Strömberg, S., Torrijos, M., Van Eekert, M., Van Lier, J., Wedwitschka, H., Wierinck, I., 2016.
627 Towards a standardization of biomethane potential tests. *Water Sci. Technol.* 74, 2515–2522.
628 <https://doi.org/10.2166/wst.2016.336>

629 Jordan, A., Cerdá, A., 2010. Actualización en métodos y técnicas para el estudio de los suelos afectados
630 por incendios forestales, in: València, U. de (Ed.), *Actualización En Métodos y Técnicas Para El*
631 *Estudio de Los Suelos Afectados Por Incendios Forestales*. FUEGORED.

632 Karthikeyan, O.P., Visvanathan, C., 2013. Bio-energy recovery from high-solid organic substrates by dry
633 anaerobic bio-conversion processes: A review. *Rev. Environ. Sci. Biotechnol.* 12, 257–284.
634 <https://doi.org/10.1007/s11157-012-9304-9>

635 Klute, A., 1986. Water Retention: laboratory methods. *Methods of soils analysis. Part 1. Physical and*
636 *minerological methods*. pp. 635–662.

637 Koch, K., Lübken, M., Gehring, T., Wichern, M., Horn, H., 2010. Biogas from grass silage -
638 Measurements and modeling with ADM1. *Bioresour. Technol.* 101, 8158–8165.
639 <https://doi.org/10.1016/j.biortech.2010.06.009>

640 Kusch, Sigrid, Kusch, S, Hans Oechsner, al, Jungbluth, T., 2012. Effect of various leachate recirculation
641 strategies on batch anaerobic digestion of solid substrates. *Int. J. Environ. Waste Manag.* 1 J.
642 *Environ. Waste Manag.* 9, 69–88. <https://doi.org/10.1504/IJEWM.2012.044161>

643 Lam, P.S., Sokhansanj, S., Bi, X., Lim, C.J., Naimi, L.J., Hoque, M., Mani, S., Womac, A.R., Ye, X.P.,
644 S., N., 2008a. Bulk density of wet and dry wheat straw and switchgrass particles. *Appl. Eng. Agric.*
645 24, 351–358. <https://doi.org/10.13031/2013.24490>

646 Lam, P.S., Sokhansanj, S., Bi, X., Mani, S., Lim, C.J., Womac, A.R., Hoque, M., Peng, J., JayaShankar,
647 T., Naimi, L.J., Nayaran, S., 2008b. Physical characterization of wet and dry wheat straw and
648 switchgrass – bulk and specific density. *ASABE Annu. Int. Meet.* 0300, 23.
649 <https://doi.org/10.13031/2013.24490>

650 Lavelle, P., Moreira, F., Spain, A., 2014. Biodiversity: Conserving biodiversity in agroecosystems.
651 *Agric. food Syst.*

652 Luxmoore, R.J., 1980. Micro-, Meso-, Macroporosity of Soil. *Environ. Sci. Div.* TN 37830, 671.

653 Menéndez, I., Caniego, J., Gallardo, J.F., Olechko, K., 2005. Use of fractal scaling to discriminate
654 between and macro- and meso-pore sizes in forest soils, in: *Ecological Modelling*. pp. 323–335.
655 <https://doi.org/10.1016/j.ecolmodel.2004.04.009>

656 Meng, X., Foston, M., Leisen, J., Demartini, J., Wyman, C.E., Ragauskas, A.J., 2013. Determination of
657 porosity of lignocellulosic biomass before and after pretreatment by using Simons' stain and NMR
658 techniques. *Bioresour. Technol.* 144, 467–476. <https://doi.org/10.1016/j.biortech.2013.06.091>

659 Møller, H.B., Moset, V., Brask, M., Riis Weisbjerg, M., Lund, P., 2014. Feces composition and manure
660 derived methane yield from dairy cows: Influence of diet with focus on fat supplement and
661 roughage type. *Atmos. Environ.* 94, 36–43. <https://doi.org/10.1016/j.atmosenv.2014.05.009>

662 Myint, M.T., Nirmalakhandan, N., 2008. Enhancing anaerobic hydrolysis of cattle manure in leach bed
663 reactors. *Bioresour. Technol.* 100, 1695–1699. <https://doi.org/10.1016/j.biortech.2008.09.031>

664 Nishiyama, N., Yokoyama, T., 2017. Permeability of porous media: Role of the critical pore size. *J.*
665 *Geophys. Res. Solid Earth* 122, 6955–6971. <https://doi.org/10.1002/2016JB013793>

666 Richards, L.A., 1948. Porous plate apparatus for measuring moisture retention and transmission by soil.
667 *Soil Sci.* 66, 105–110.

668 Riggio, S., Hernández-Shek, M.A., Torrijos, M., Vives, G., Esposito, G., Van Hullebusch, E.D., Steyer,
669 J.P., Escudié, R., 2017a. Comparison of the mesophilic and thermophilic anaerobic digestion of
670 spent cow bedding in leach-bed reactors. *Bioresour. Technol.* 234, 466–471.
671 <https://doi.org/10.1016/j.biortech.2017.02.056>

672 Riggio, S., Torrijos, M., Debord, R., Esposito, G., van Hullebusch, E.D., Steyer, J.P., Escudié, R., 2017b.
673 Mesophilic anaerobic digestion of several types of spent livestock bedding in a batch leach-bed
674 reactor: substrate characterization and process performance. *Waste Manag.* 59, 129–139.
675 <https://doi.org/10.1016/j.wasman.2016.10.027>

676 Rocamora, I., Wagland, S.T., Villa, R., Simpson, E.W., Fernández, O., Bajón-Fernández, Y., 2020. Dry
677 anaerobic digestion of organic waste: A review of operational parameters and their impact on
678 process performance. *Bioresour. Technol.* 299, 122681.
679 <https://doi.org/10.1016/j.biortech.2019.122681>

680 Sanchez, A., Hernández-Sánchez, P., Puente, R., 2019. Hydration of lignocellulosic biomass. Modelling
681 and experimental validation. *Ind. Crops Prod.* 131, 70–77.
682 <https://doi.org/10.1016/j.indcrop.2019.01.029>

683 Savitzky, A., Golay, M.J.E., 1964. Smoothing and Differentiation of Data by Simplified Least Squares
684 Procedures. *Anal. Chem.* 36, 1627–1639. <https://doi.org/10.1021/ac60214a047>

685 Sawatdeenarunat, C., Surendra, K.C., Takara, D., Oechsner, H., Khanal, S.K., 2015. Anaerobic digestion
686 of lignocellulosic biomass: Challenges and opportunities. *Bioresour. Technol.* 178, 178–186.
687 <https://doi.org/10.1016/j.biortech.2014.09.103>

688 Shahriari, H., Warith, M., Hamoda, M., Kennedy, K.J., 2011. Effect of leachate recirculation on
689 mesophilic anaerobic digestion of food waste. *Waste Manag.* 32, 400–403.
690 <https://doi.org/10.1016/j.wasman.2011.10.022>

691 Shewani, A., Horgue, P., Pommier, S., Debenest, G., Lefebvre, X., Gandon, E., Paul, E., 2015.
692 Assessment of percolation through a solid leach bed in dry batch anaerobic digestion processes.
693 *Bioresour. Technol.* 178, 209–216. <https://doi.org/10.1016/j.biortech.2014.10.017>

694 Valencia, R., Van Der Zon, W., Woelders, H., Lubberding, H.J., Gijzen, H.J., 2008. The effect of
695 hydraulic conditions on waste stabilisation in bioreactor landfill simulators. *Bioresour. Technol.*
696 100, 1754–1761. <https://doi.org/10.1016/j.biortech.2008.09.055>

697 Vallabh, R., Ducoste, J., Seyam, A.F., Banks-Lee, P., 2011. Modeling tortuosity in thin fibrous porous
698 media using computational fluid dynamics. *J. Porous Media* 14, 791–804.

699 <https://doi.org/10.1615/JPorMedia.v14.i9.40>

700 Van Soest, P.J., 1963. Use of Detergents in the Analysis of Fibrous Feeds. II. A Rapid Method for the
701 Determination of Fiber and Lignin. *J. Assoc. Off. Agric. Chem.* 46, 825–835.

702 Wassar, F., Gandolfi, C., Rienzner, M., Chiaradia, E.A., Bernardoni, E., 2016. Predicted and measured
703 soil retention curve parameters in Lombardy region north of Italy. *Int. Soil Water Conserv. Res.* 4,
704 207–214. <https://doi.org/10.1016/j.iswcr.2016.05.005>

705 Yokoyama, T., Takeuchi, S., 2009. Porosimetry of vesicular volcanic products by a water-expulsion
706 method and the relationship of pore characteristics to permeability. *J. Geophys. Res. Solid Earth*
707 114. <https://doi.org/10.1029/2008JB005758>

708

709 **Figures**

710 **Fig. 1 (a)** Schematic pores structure of the biomass and definitions of pores function **(b)**

711 Theoretical WRC with the test phases: Immersion and saturation (I&S), Drainage analysis (DA)

712 and Thermogravimetric analysis (TGA)

713 **Fig. 2** Savitzky-Golay filter derivation over time of TGA results for RSG

714 **Fig. 3** WRC and porosity distribution for **(a)** Roadside grass (RSG), **(b)** Chopped corn stover

715 (CCS) **(c)** Cattle Manure (CM) and **(d)** Shredded Cattle Manure (S-CM)

716 **Fig. 4 (a)** Specific biogas and methane flow in 60 L sacrificed batch reactors **(b)** Accumulated

717 methane

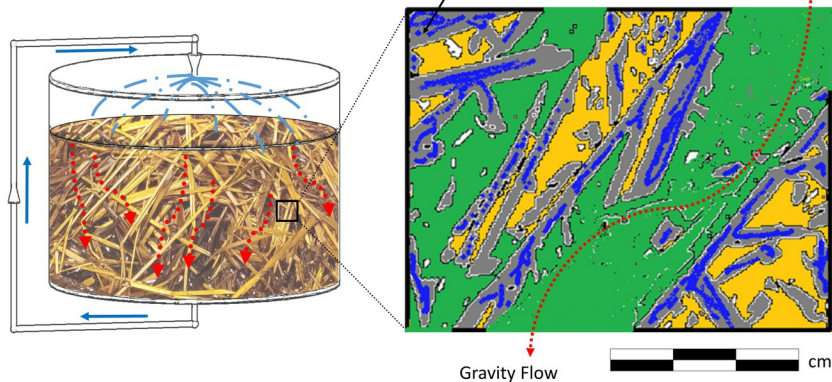
718 **Fig. 5 (a)** WRC for CM treated in 60 L LBR's **(b)** Porosity distribution evolution of CM

719 anaerobically digested

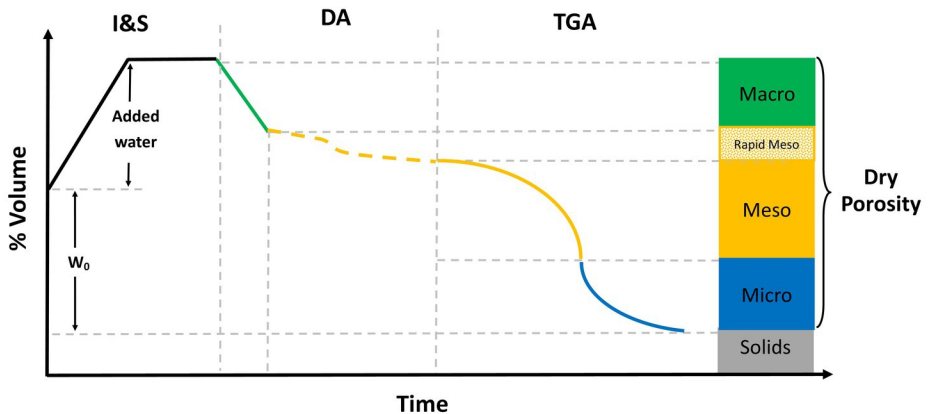
720 **Fig. 6 (a)** Fiber content degradation of CM **(b)** Permeability changes of CM **(c)** Reduction of

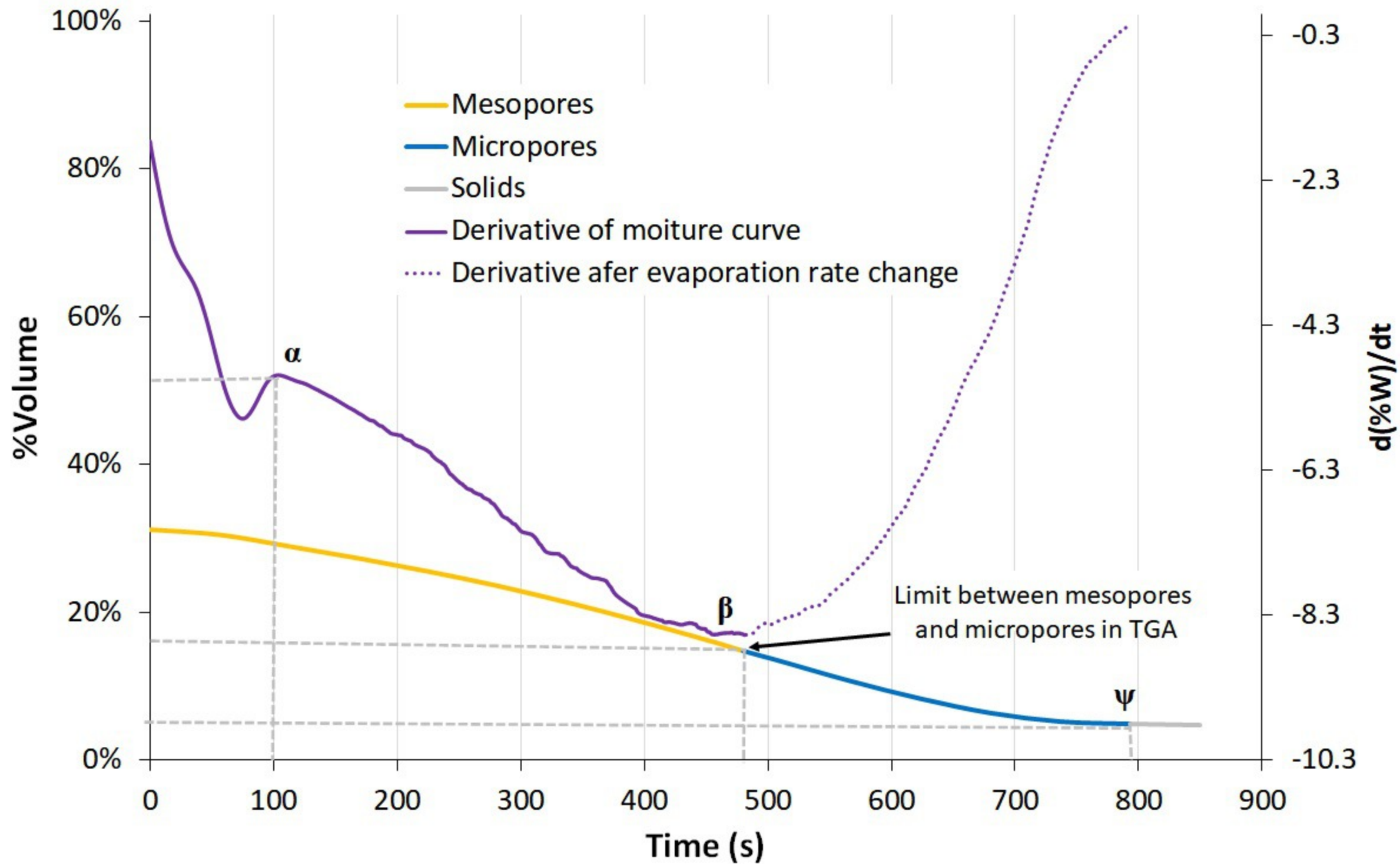
721 daily recirculated volume with macropores evolution in D-AD

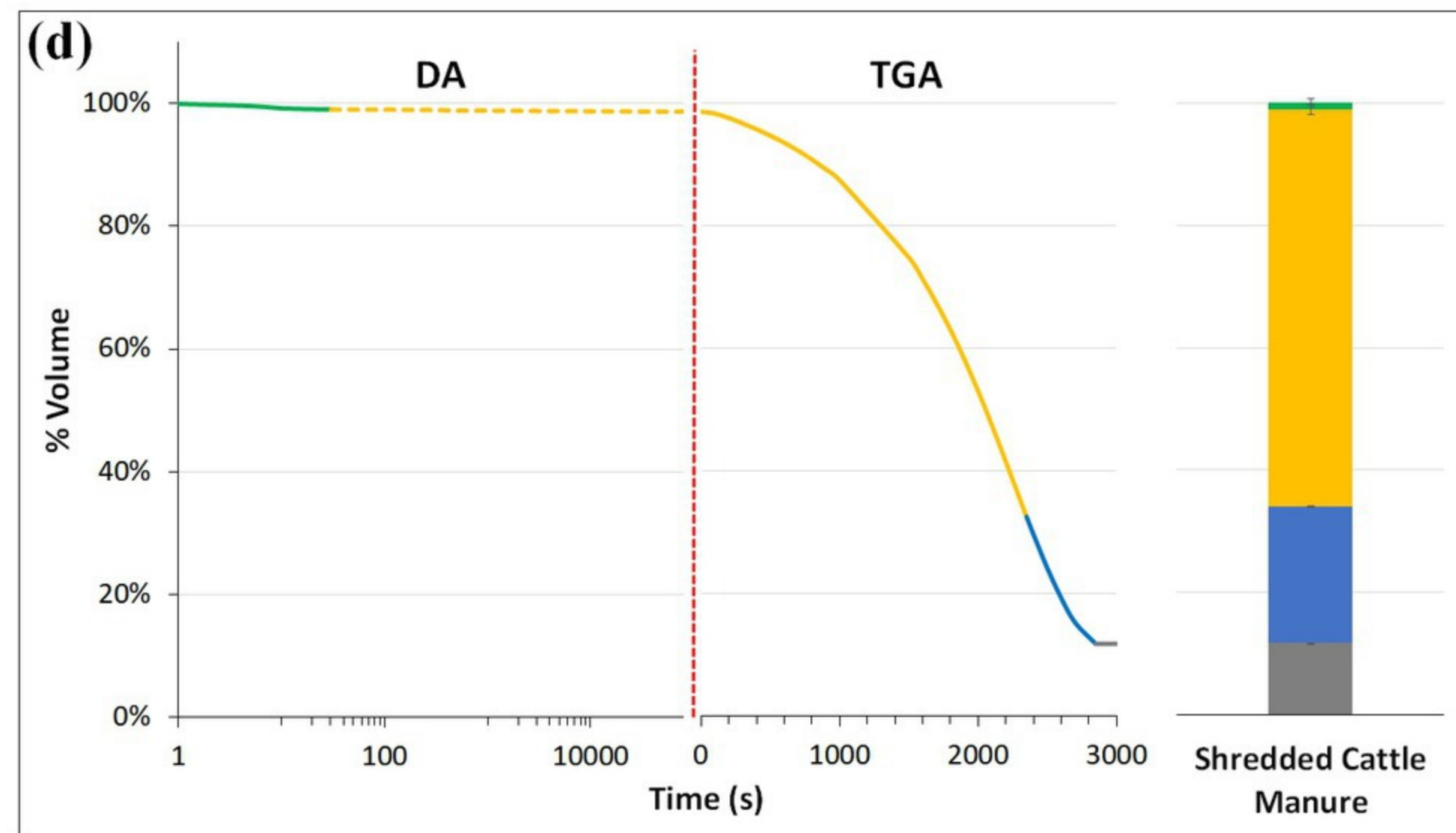
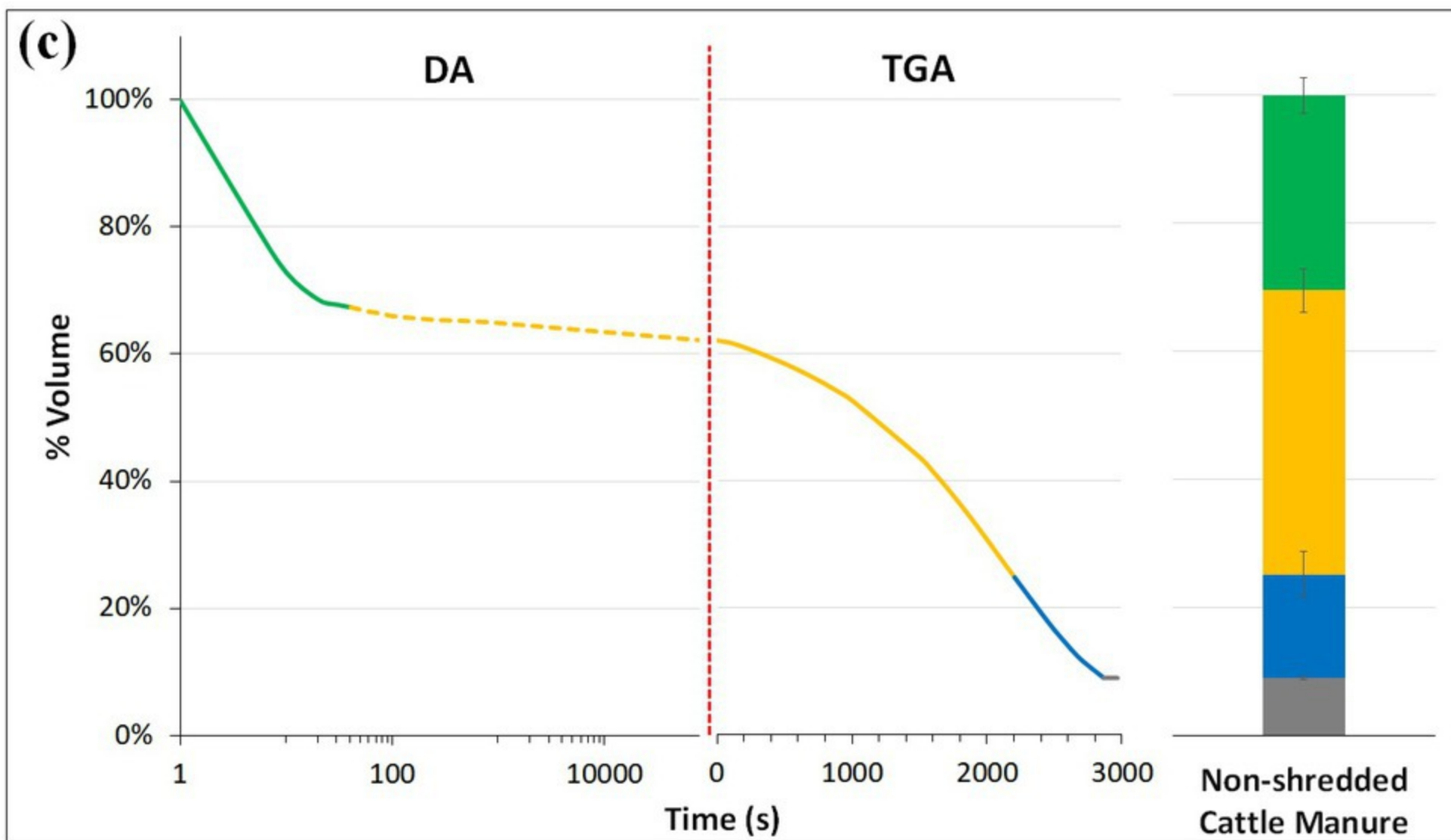
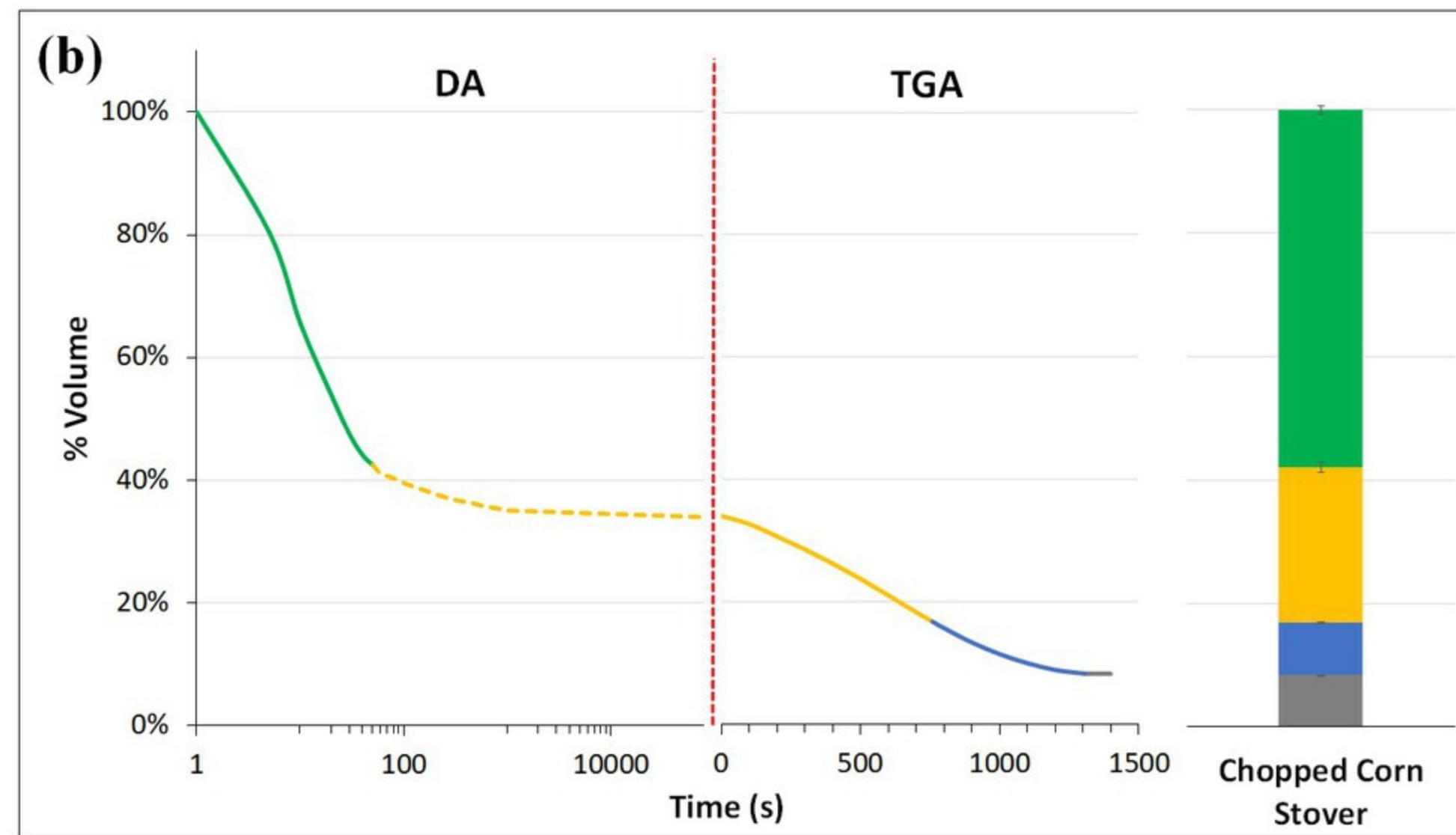
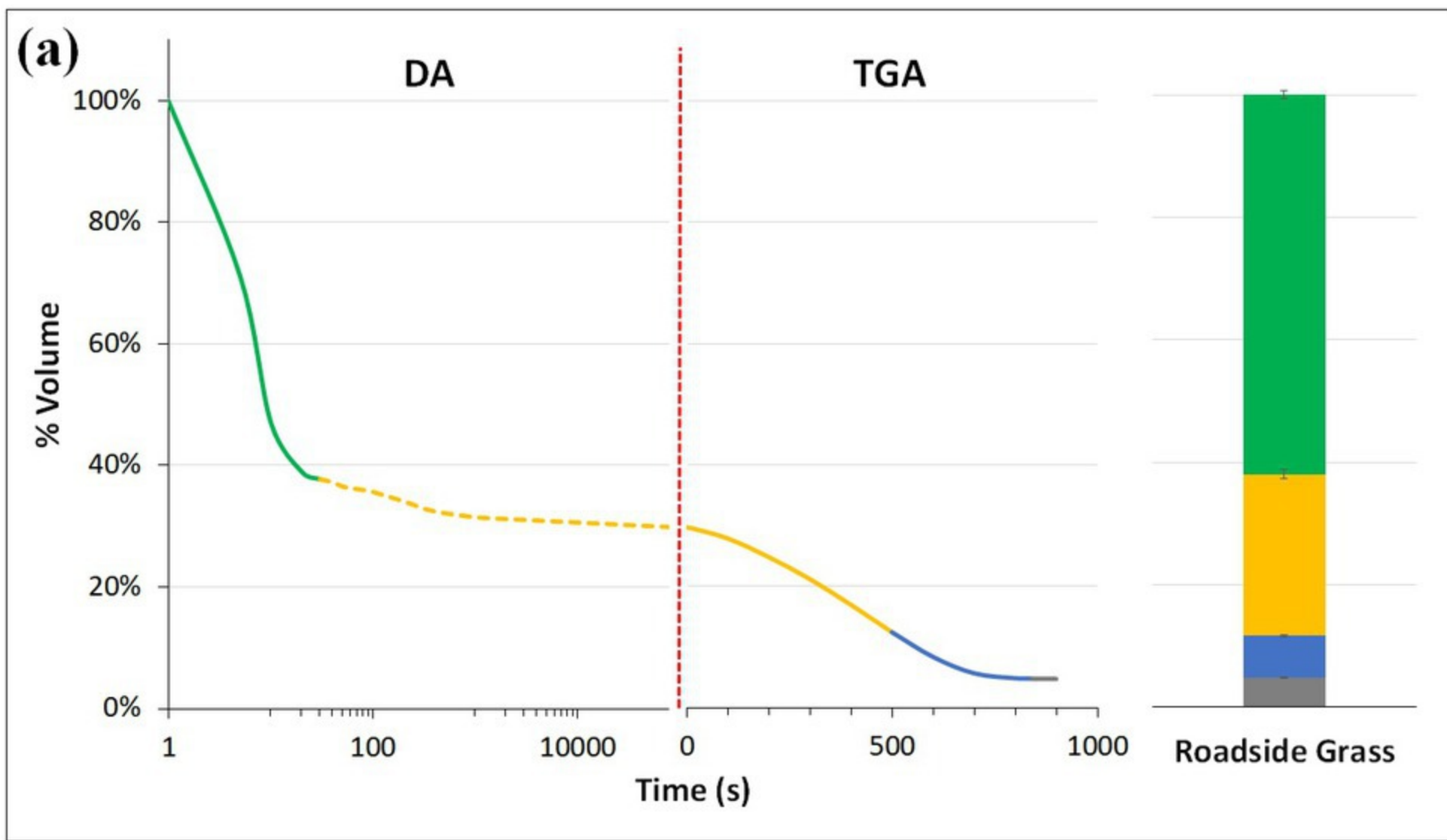
722

(a)**Leach Bed Reactor (LBR)****Pores classification according to their size and function :**

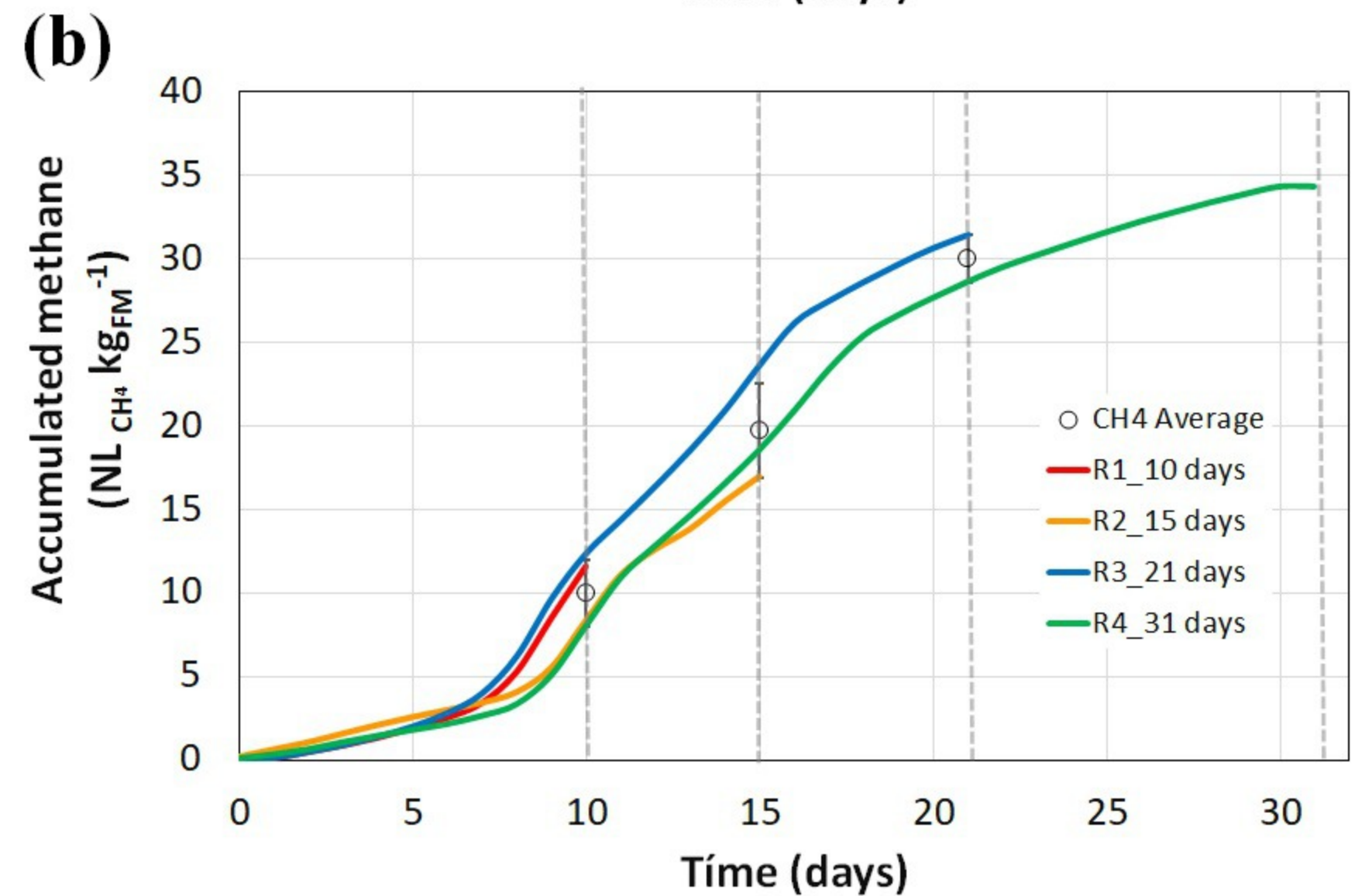
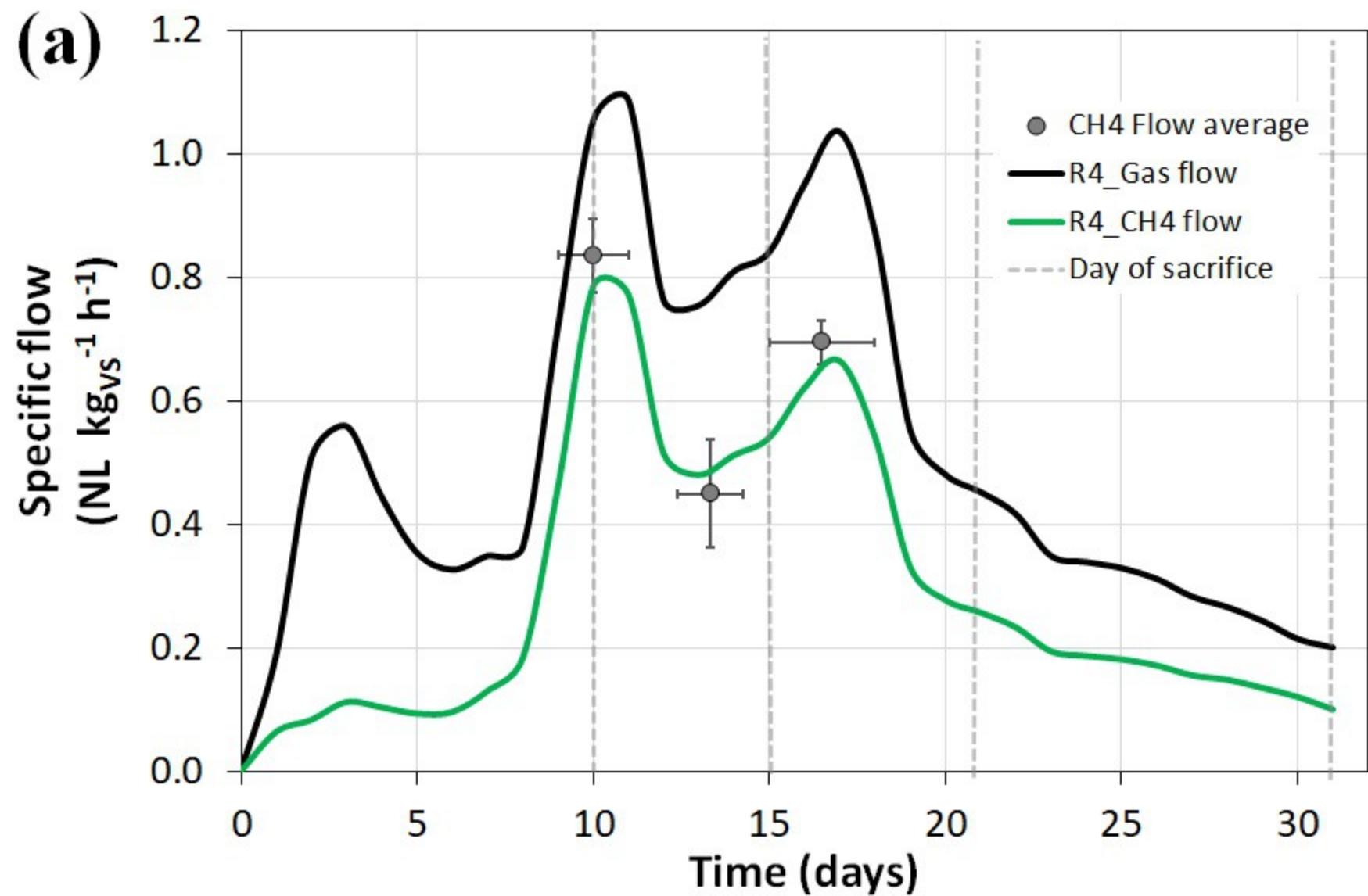
- Macropores: (> 1 mm)**
Gas phase and drainage (gravity flow)
- Mesopores: (10 μm - 1 mm)**
Water conduction (capillary flow)
- Micropores: (< 10 μm)**
Hygroscopic water retention

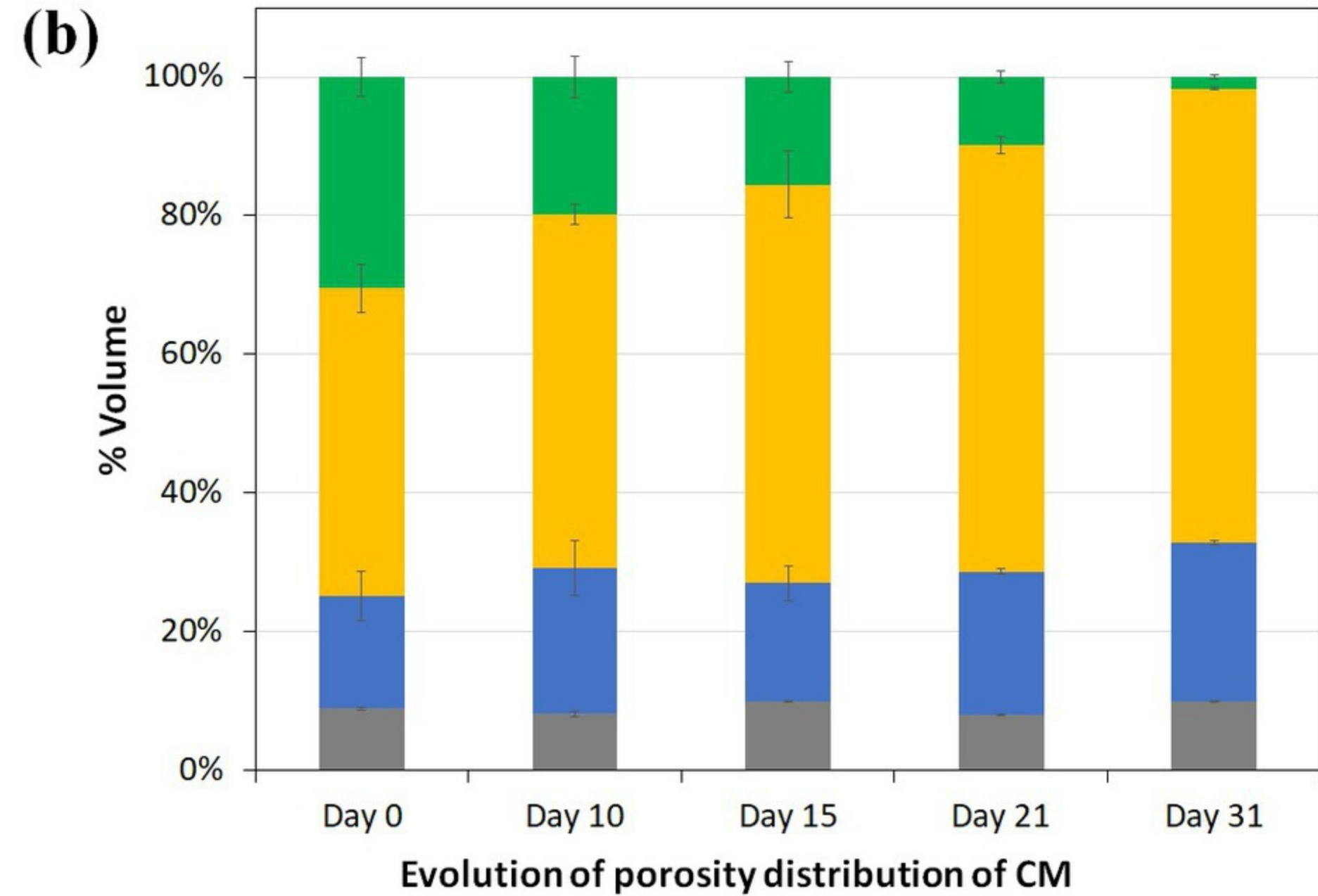
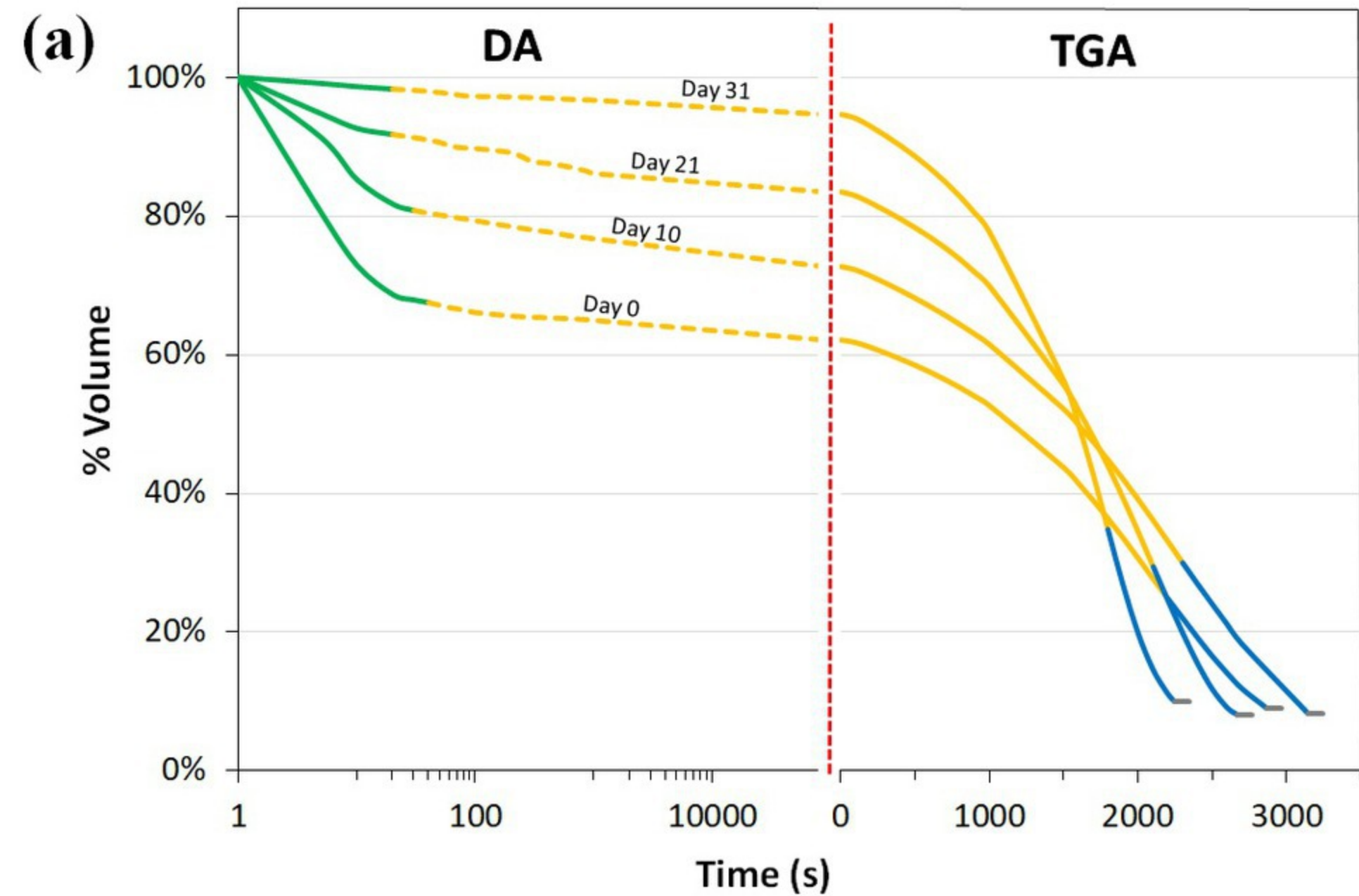
(b)





■ Macropores ■ Mesopores ■ Macropores ■ Solids





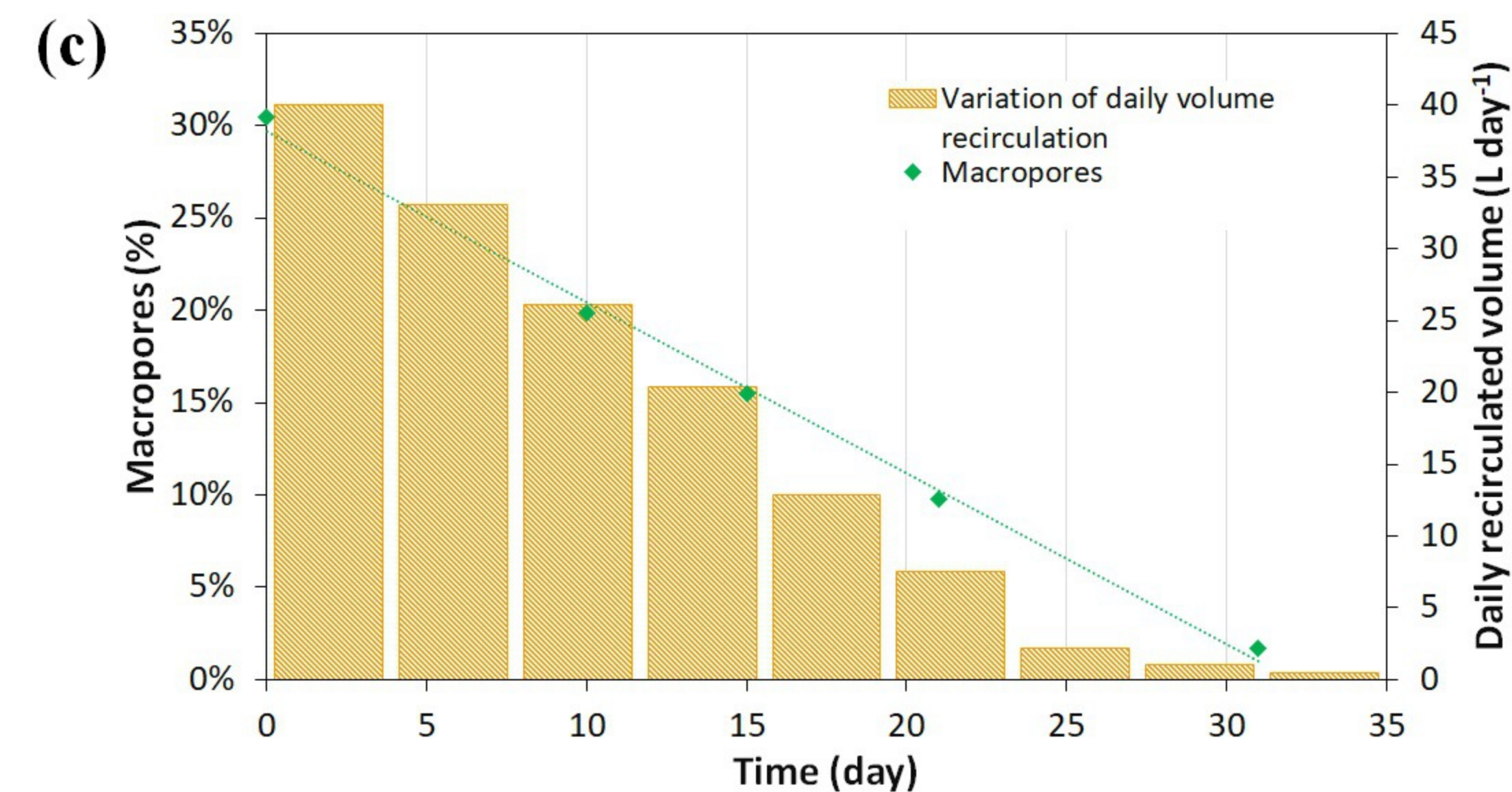
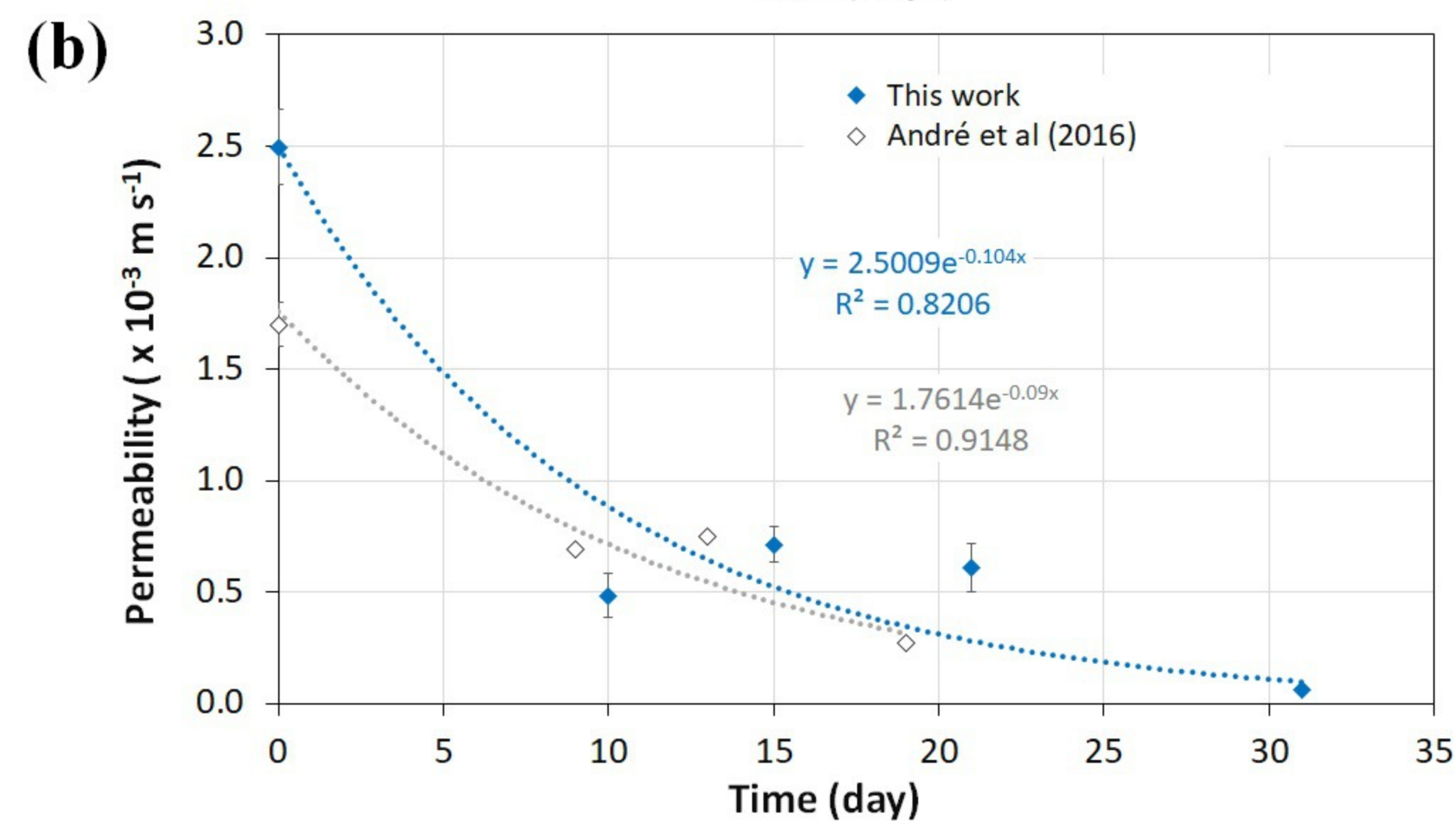
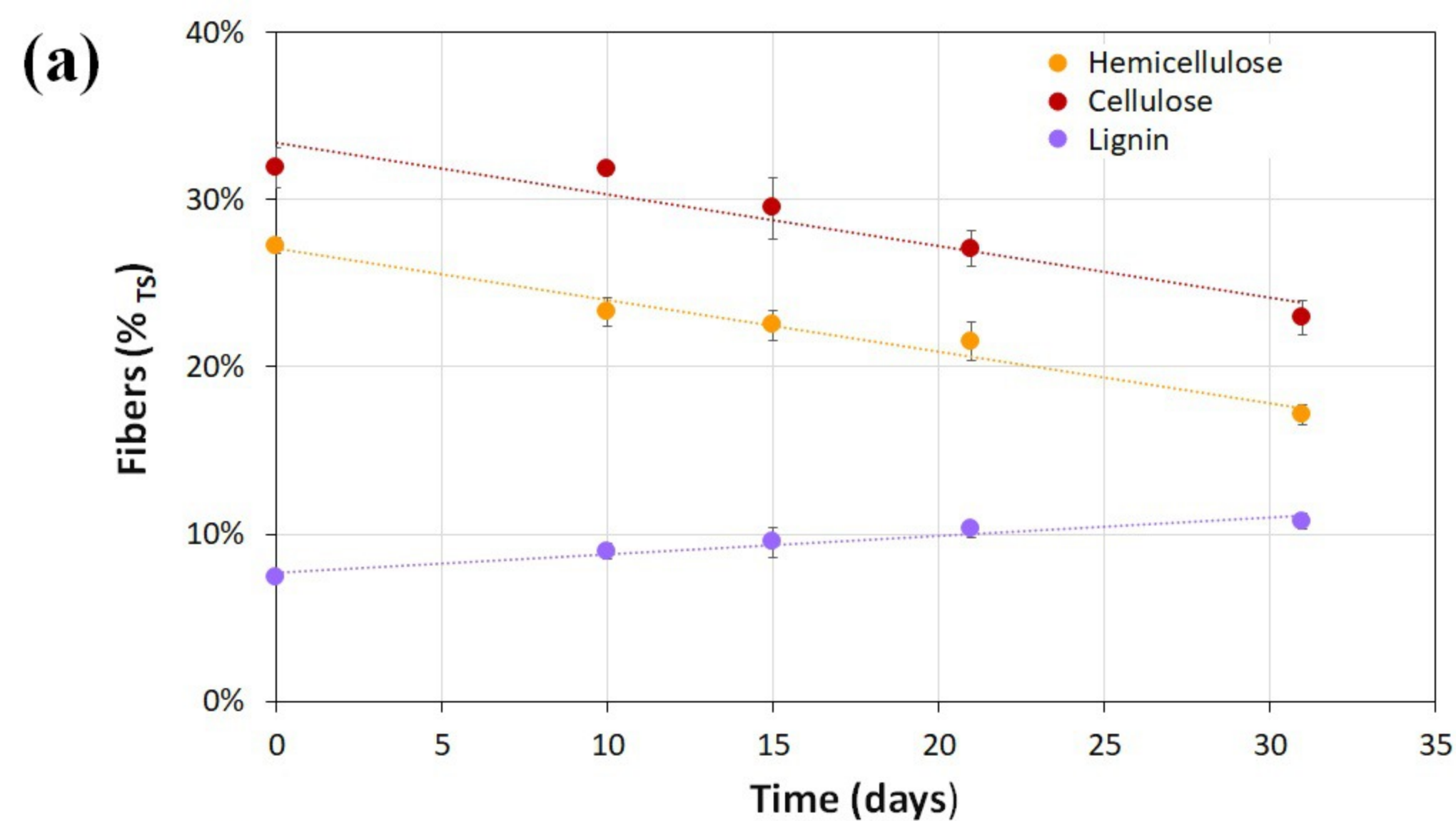


Table 1. Biomass characterization

Biomass	RSG	CCS	S-CM	CM
Particle shape	Plate	Angular	Plate	Cylindrical
Particle size	Length: 10-15 cm Thickness: <2 mm	1-2 cm	Length: <5 cm Thickness: <2 mm	Length: 10-20 cm Diameter: <5 mm
TS (%)	22.6 ± 0.6	37.9 ± 0.6	14.5 ± 1.7	18.6 ± 0.4
VS (%_{TS})	85.3 ± 0.6	95.8 ± 0.7	79.4 ± 1.5	86.4 ± 0.1
ρ_{wet} (kg m⁻³)	174.1 ± 4.5	166.2 ± 0.7	797.8 ± 11.4	407.8 ± 14.1
ρ_{dry} (kg m⁻³)	39.4 ± 1.0	63.0 ± 0.3	115.6 ± 1.7	75.8 ± 2.6
ϵ_{wet} (%)	78.7 ± 0.1	77.9 ± 0.4	18.6 ± 1.7	51.7 ± 1.3
ϵ_{dry} (%)	95.2 ± 0.1	91.6 ± 0.1	88.2 ± 0.3	91.0 ± 0.2
$\theta_{\text{mobile}} / \theta_{\text{added}}$ (%)	76.1 ± 0.8	73.7 ± 2.3	5.5 ± 1.0	60.0 ± 3.6
$\theta_{\text{mobile}} / \theta_{\text{total}}$ (%)	62.9 ± 0.6	62.6 ± 2.2	1.2 ± 0.1	33.5 ± 2.7
WHC (g_{water} g_{DM}⁻¹)	7.4 ± 0.1	4.1 ± 0.2	7.4 ± 0.2	6.7 ± 0.2
WMB (%)	96.7 ± 0.1	99.0 ± 0.8	99.0 ± 0.2	98.5 ± 2.2
K (m s⁻¹)	1.3 ± 0.3 · 10 ⁻³	8.6 ± 0.6 · 10 ⁻⁴	1.2 ± 0.2 · 10 ⁻⁸	2.5 ± 0.2 · 10 ⁻³

Table 2. Physical characteristics evolution of digested CM

Event	CM_Day 0	CM_Day 10	CM_Day 15	CM_Day 21	CM_Day 31
TS (%)	18.6 ± 0.4	11.7 ± 0.1	13.9 ± 0.1	10.5 ± 0.3	11.1 ± 0.5
VS (%_{TS})	86.4 ± 0.1	82.7 ± 0.2	82.1 ± 0.3	78.6 ± 0.2	76.0 ± 0.3
ρ_{wet} (kg m⁻³)	407.8 ± 14.1	556.0 ± 4.0	594.6 ± 13.8	766.2 ± 15.3	914.2 ± 0.9
ρ_{dry} (kg m⁻³)	75.8 ± 2.6	64.8 ± 0.5	82.9 ± 1.9	80.6 ± 1.6	101.5 ± 1.2
ϵ_{wet} (%)	51.7 ± 1.3	29.8 ± 3.2	28.4 ± 0.2	23.9 ± 1.1	10.2 ± 1.5
ϵ_{dry} (%)	91.0 ± 0.2	91.8 ± 0.4	90.0 ± 0.1	92.0 ± 0.1	90.0 ± 0.2
WHC (g_{water} g_{DM}⁻¹)	6.7 ± 0.2	8.9 ± 0.1	7.5 ± 0.3	10.4 ± 0.3	8.9 ± 0.2
WMB (%)	98.5 ± 2.2	95.1 ± 0.1	95.3 ± 4.6	88.3 ± 1.3	96.6 ± 0.7

Table 3. Evolution of linear regression parameters for CM treated in sacrificed batch

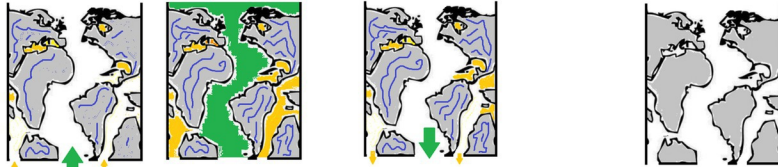
LBR's

	Parameter (y)	m	y₀	R²
Porosity distribution (% Total volume)	Macropores	-0.0090	0.2945	0.99
	Mesopores	0.0068	0.4529	0.96
	Micropores	0.0019	0.1665	0.61
Fiber content (%TS)	Hemicellulose	-0.0310	0.2705	0.97
	Cellulose	-0.0031	0.3337	0.89
	Lignin	0.0110	0.0772	0.95
Compaction	Height (m)	-0.0081	0.4026	0.93
	Wet bulk density (kg m⁻³)	16.69	390.76	0.98

Table 4. Results linear regression comparing the results of characterization of digested

CM

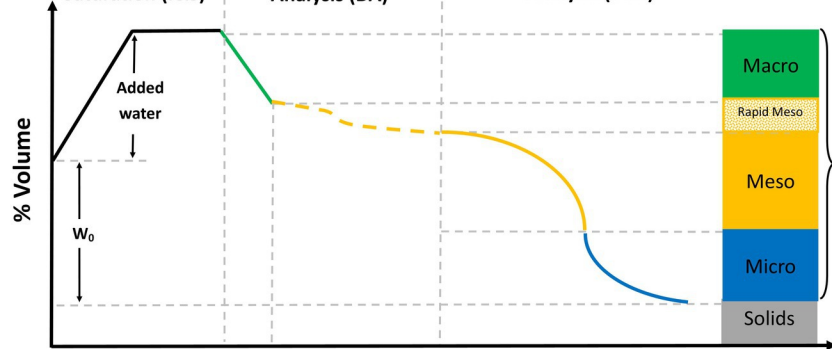
Parameters	Coefficient R	p-value	Confidence level
VS ↔ Hemicellulose	0.97	$6.17 \cdot 10^{-3}$	95%
VS ↔ Cellulose	0.94	$1.94 \cdot 10^{-2}$	95%
Hemicellulose ↔ Macropores	0.98	$2.56 \cdot 10^{-3}$	95%
Cellulose ↔ Macropores	0.93	$2.36 \cdot 10^{-2}$	95%
Macropores ↔ Solid Height	0.98	$4.37 \cdot 10^{-3}$	95%
Macropores ↔ Permeability	0.87	$5.56 \cdot 10^{-2}$	90%



Immersion and Saturation (I&S)

Draining Analysis (DA)

Thermogravimetric Analysis (TGA)



Biomass pore classification

- **Macropores: (> 1 mm)**
Gas phase and drainage (gravity flow)
- **Mesopores: (10 μm - 1 mm)**
Water conduction (capillary flow)
- **Micropores: (< 10 μm)**
Hygroscopic water retention

Dry Porosity

Macro

Rapid Meso

Meso

Micro

Solids